View metadata, citation and similar papers at core.ac.uk

brought to you by CORE

provided by Apollo

Benchmarking the Timmins Process – a novel approach for low energy pre-combustion carbon capture in IGCC flowsheets.

Bart Hallmark[*†], *Julian Parra-Garrido*[‡], *Andrew Murdoch*[†], *Ian Salmon*[‡] *and Chris Hodrien*[§]

[†]Department of Chemical Engineering and Biotechnology, University of Cambridge, New Museums Site, Pembroke St., Cambridge. CB2 3RA

[‡]Jacobs UK Limited, 1 Port Way, Port Solent, Portsmouth PO6 4TY.

Email: Ian.Salmon@jacobs.com

[§]Timmins CCS Ltd., The Manor House, School Street, Woodford Halse, Northamptonshire, NN11 3RL

Email: chodrien@blueyonder.co.uk

KEYWORDS: Clean coal technologies, Modelling and simulation studies

[*]Corresponding author, Email: bh206@cam.ac.uk

ABSTRACT

This paper reports results from an initial benchmarking study of the Timmins Process, a novel pre-combustion carbon capture process that uses a combination of traditional unit operations, DEPG scrubbing, carbon monoxide shift and carbon dioxide liquefaction, in a unique arrangement. The study examines the performance of the Timmins Process embedded within an integrated gasifier combined cycle (IGCC) flowsheet and the results are compared to data from the US Department of Energy (DoE) cost and performance baseline studies for coal-fired energy plants. Modeling was undertaken using UniSim R400 (Honeywell Inc.) with thermodynamic parameters for DEPG interactions being regressed from literature data; these results are also reported here. The net efficiency of an IGCC flowsheet incorporating the Timmins Process, with a carbon capture level of 91.8 % on a mass basis, varies between 33.8 % and 34.3 % depending on the process configuration and the cooling water temperature. This result compares very favorably to a DoE study for a conventional capture process embedded within an IGCC flowsheet that operated at an efficiency of 31.2 %. Further, more detailed, studies are recommended to assess the impact of various assumptions that underpin this work.

INTRODUCTION

Carbon capture and storage (CCS) has been a major research focus, both academically and industrially, for a number of years since it is a way in which fossil fuel-based energy production can be maintained but with a significant reduction in carbon dioxide emissions[1, 2]. In 2009, 67.1 % of world electricity generation, almost 13,500 TWh, was derived from the combustion of fossil fuels[3]: a clear incentive exists, therefore, for emission reduction in the power generation sector.

CCS methodologies typically comprise three steps: capture, transportation and storage. Storage can take the form of either geological storage, such as injection into depleted oil or gas reservoirs, oceanic sequestration or mineralization. Much literature exists on this subject[2] and, as such, will not be considered any further in this paper. Carbon capture in the context of power plants can be undertaken using one of three general approaches; post-combustion capture, pre-combustion capture and oxy-fuel combustion[2, 4]. The efficiency of carbon capture schemes vary depending on the nature of the fuel source and combustion scheme along with the percentage of carbon dioxide captured. For example, post-capture schemes have projected plant efficiencies between 42.8 % for a natural gas combined cycle with amine scrubbing (US Department of Energy (DoE) baseline studies, case 14)[5] and 26.2 % for a subcritical pulverized coal power plant also equipped with amine scrubbing (DoE Case 10)[5]. These efficiency figures represent a carbon capture level of 90 % on a mass basis and are referenced against the higher heating value (HHV) of the fuel source.

The parasitic energy load of post-capture processes is significant, as revealed when the efficiency data for the pulverized coal power plant equipped with amine scrubbing is compared to a similar process that is not equipped with carbon capture. According to DoE figures[5], the overall plant efficiency drops by 28.8 %; for a unit exporting 550 MWe, this corresponds to an increase in required gross power output from 582 MWe to 672 MWe.

In the oxy-fuel approach, combustion is performed with pure oxygen. This stream of oxygen is produced using either cryogenic air separation or membranes[6]; the air separation represents one of the main costs of the technology[2]. A key advantage of this process is that the combustion product consists primarily of carbon dioxide and water with some authors[7] reporting that the concentration of carbon dioxide in the output stream is above 80 % v/v. Other authors have indicated that this concept produces significant amounts of water and that excess oxygen and argon

are present alongside the carbon dioxide; consequently the effort needed for carbon dioxide purification still remains high[8]. When the oxy-fuel approach is applied to novel coal-fired power station flowsheets, specifically Integrated Gasification Combined Cycle (IGCC) plants, the approach shows a potentially high efficiency, up to 45.7 % (based on the lower heating value of the fuel), with 96 % v/v of carbon dioxide being captured[8]. A potential problem with the IGCC oxy fuel approach is a high level of technical risk, a potentially high level of plant complexity and the amount of research that still needs to be undertaken[8].

In solid fuel pre-combustion capture systems, for example IGCC with CCS, solid fuel is gasified by oxygen and/or steam and then shift converted to form a mixture of hydrogen and carbon dioxide; the carbon dioxide is then separated from the fuel before it is burned[4], [8]. An advantage of this approach is the relatively high partial pressure and concentration of carbon dioxide that is attained: about 10–12 bar and 40 % v/v respectively[4], [9]. The high carbon dioxide concentration in the gas stream allows efficient de-carbonization of the fuel *via* established scrubbing processes[10]: the scrubbing equipment is typically smaller and physical solvents can be used resulting in the process having a lower overall energy usage when compared to post-combustion capture[2]. A block diagram of a typical pre-combustion power plant is shown in Figure 1[11].

Pre-combustion carbon capture schemes normally use physical solvents, for instance methanol (Rectisol®), n-methyl-2-pyrolydone (Purisol®) or a mixture of dimethyl ethers of polyethylene glycol (DEPG or Selexol®)[9]. Some researchers have reported that DEPG processes are the most energy efficient commercially-available acid gas removal systems[4]. Other independent research has compared DEPG and methanol and reported similar results; the DEPG process is less costly than the methanol process for fuel-cycle carbon dioxide capture[12]. Furthermore, additional research[13] has emphasized that DEPG has a clear advantage over other physical and chemical solvents in all scrubbing applications that remove hydrogen sulfide and carbon dioxide from hydrocarbon systems. One disadvantage of the methanol-based process is that it requires deep refrigeration of the solvent as a consequence of the high vapor pressure of methanol; temperature between −40 °C and −60 °C are typically used. This tends to result in a more complex flowsheet compared to other processes that employ physical solvents[4]. Contrastingly, an advantage of the DEPG-based process is that refrigeration not required due to DEPG's low vapor pressure (0.00073 mm Hg at 25 °C[13]). Moreover, thermal solvent regeneration is not required with DEPG regeneration being achieved solely by pressure reduction[4].

As with other capture schemes, the efficiency of pre-capture depends on the exact configuration of the process flowsheet, but typical figures for coal-fired IGCC schemes range between 32.6 % to 31.2 % (DoE cases 2 and 6 respectively)[5]. These efficiencies are measured at 90 % carbon capture (on a mass basis) and use the HHV of the fuel source. The level of technical risk, plant complexity and further research required for pre-capture IGCC schemes varies considerably[8].

A new approach, the Timmins Process, for capturing carbon from IGCC power plants has been recently proposed[14]–[16]. This process combines industrially-proven unit operations arranged in a novel configuration to lower the technical risk of pre-capture processes. Preliminary indications[14]–[16] suggest that the Timmins Process could also have a high efficiency when compared to other IGCC pre-capture schemes due to its use of DEPG as a solvent at gasifier pressure (36 bara) as opposed to atmospheric pressure, its use of cryogenic carbon dioxide liquefaction and pumping to export pressure as opposed to the use of gas compression and its novel sequence of processing steps. A block diagram of the Timmins Process, showing typical process conditions and stream compositions, is shown in Figure 2.

This paper reports results from the first benchmarking study of the Timmins Process. A critical factor in the validity of this feasibility study was the development and verification of a thermodynamic model for gas dissolution within DEPG solvent, and of the behavior of gas mixtures under cryogenic conditions. These thermodynamic models are presented and discussed prior to introducing the detailed process simulation work, which it underpins. Process simulation of both the capture process and of the IGCC power island was carried out using UniSim Design R400 (Honeywell Inc.) such that the energy consumption and overall efficiency of the Timmins Process can be rigorously assessed and compared to existing literature on IGCC power schemes[5]. The key assumptions that were made during process modeling are summarized in Table 1; this Table also indicates the likely impact of these assumptions on the modelling results. A number of these assumptions are discussed in more detail in the sections that follow. The finalized process model will also allow the sensitivity of the Timmins Process to be evaluated with respect to changes in utility supply, such as cooling water temperature.

THERMODYNAMIC BASIS

Establishing an accurate thermodynamic basis is fundamental to any study that involves process simulation. The Timmins Process contains two plant areas where careful validation of the chosen

thermodynamic model is important; the first is the prediction of gas solubility in DEPG and the second is the behavior of liquefied gas mixtures.

Modeling DEPG Behavior

A key challenge when modeling processes that use DEPG as a physical solvent is the lack of vapor liquid equilibrium data in the open literature due to the proprietary nature of the DEPG mixtures used. Two important studies that are openly available establish the solubility of carbon dioxide and hydrogen sulfide as a function of temperature in DEPG at atmospheric pressure[17], and the solubility ratio of nitrogen, hydrogen, carbon monoxide and methane with respect to carbon dioxide in DEPG[18] at atmospheric pressure and 25 °C. These data were used in the current research to obtain estimates of Henry's law parameters that could be used with a suitable activity coefficient model to describe the behavior of non-condensable gases within UniSim Design R400.

Henry's law parameters are obtained by examining the relationship between the concentration of a gaseous component, *i*, in the vapor phase, y_i, and its corresponding concentration in the liquid phase, x_i. This relationship is typically a function of pressure, $\mathcal{P}$, and the Henry's coefficient, H_{ij}, between the gaseous phase, *i*, and the liquid phase into which the gas is dissolving, *viz*:

$$x_i = \frac{y_i P}{H_{ij}} \tag{1}$$

Typically, the Henry's coefficient is a function of temperature; UniSim Design uses the extended Henry's law equation[19] to model this dependence:

$$\ln H_{ij} = A + \frac{B}{T} + C\ln(T) + DT \tag{2}$$

In Equation (2), *A*, *B*, *C* and *D* correspond to Henry's law interaction parameters and T is the temperature in Kelvin. Experimental data presented in the open literature[17] describe the temperature dependence of Henry's coefficient for carbon dioxide and hydrogen sulfide in DEPG at atmospheric pressure. These data are plotted as individual data points in the plot shown in Figure 3 and allow for the regression of *A* and *B* in Equation (2).

In order to obtain the approximate behavior of other syngas components, specifically nitrogen, methane, hydrogen and carbon monoxide, in DEPG at elevated temperature it was assumed that

the temperature dependence of the Henry's law coefficient followed the same trend as the carbon dioxide and hydrogen sulfide data whilst maintaining relative solubility values consistent with literature data at 25 °C. Whilst the chemical nature of the species in the system under study may mean that these assumptions are not entirely representative of their behavior, this is the best that can be done given the limited nature of the information (mostly just single data points) that is available in the open literature. A similar approach has been taken by other researchers in this field[20]. The estimated dependence of the Henry's coefficient as a function of temperature for nitrogen, methane, hydrogen and carbon monoxide is shown by the continuous lines in the plot in Figure 3. Parameters *A* and *B* can be estimated from this data regression for these components; these parameters are given in Table 2 for all six components in a form that can be entered directly into the a_{ij} interaction matrix within UniSim Design[19].

Once the Henry's law parameters have been regressed, a suitable choice of thermodynamic model needs to be made. Some researchers[20] in this field have successfully used the PC-SAFT equation of state[21], but the Henry's law regression described above only applies to activity coefficient models. Consequently, the data shown in Table 2 was used in conjunction with the NRTL model[22] for this study. The predicted solubility of the five components of interest, carbon dioxide, hydrogen, carbon monoxide, nitrogen and methane, in DEPG at 30 bara ("low pressure") and 69 bara ("high pressure") was then checked against experimental literature data[18] at 25 °C and 1 atmosphere. As a comparison, solubility predictions of these components resulting from the Peng Robinson equation of state[23] were also included since Peng Robinson is sometimes recommended as a suitable thermodynamic model when dealing with non-condensable components of this nature[19]. A plot showing the deviation in predicted solubility from literature values is given in Figure 4. It must be emphasized that the Peng Robinson model was used without any additional parameter tuning, whereas the NRTL activity coefficient model had been tuned using the Henry's law parameters as already described.

It can be seen from the plot shown in Figure 4 that the NRTL activity coefficient model tuned with the Henry's law parameters given in Table 2 maintains a consistent solubility prediction at 30 bara and 69 bara when compared to experimental data at 1 atmosphere. The Peng Robinson equation of state, however, predicts solubility ratios that are significantly different from those suggested by experimental data. For this reason, the NRTL activity coefficient model with

regressed Henry's law parameters, as described above, was used for this study; further confirmation of its suitability for a study of this nature was also obtained[24].

Modeling Cryogenic Gas Mixture Behaviour

Experimental bubble point data for mixtures of carbon monoxide and nitrogen[25] and mixtures of hydrogen, carbon monoxide and carbon dioxide[26] were compared to predicted bubble points calculated by UniSim Design using the Peng Robinson equation of state[23]. Tuning of the Peng Robinson equation of state can be achieved by adjusting an experimental parameter, K_{ij}[27], that acts on the quadratic mixing term: this parameter can describe temperature dependence and contains five adjustable coefficients, as shown in Equation (3).

$$K_{ij} = \alpha_{ij} + \beta_{ij}T + \gamma_{ij}T^2 + \exp\left(\delta_{ij} + \frac{\epsilon_{ij}}{T}\right) \tag{3}$$

K_{ij} was adjusted for CO_2 for both the high and low pressure hydrogen, carbon monoxide and carbon dioxide data sets. The objective was to obtain a value of the coefficient of determination[28], R^2, greater than 0.9 for both data sets, with emphasis placed on the lower pressure data set since this is closer to the conditions found within the cryogenic section of the Timmins Process. With $\alpha_{ij} = -0.3$, $\beta_{ij} = 1 \times 10^{-4}\ \mathrm{K}^{-1}$ and $\gamma_{ij} = 7 \times 10^{-6}\ \mathrm{K}^{-2}$, R^2 values of 0.91 were obtained for the high pressure data set and 0.97 for the low pressure data set. Plots showing the comparison between experimental data and UniSim prediction are given in Figure 5 and Figure 6 respectively; the discrete data points shown in the inset in Figure 6 illustrate the pressures and temperatures of all streams within the cryogenic unit of the Timmins process.

As can be seen from the data shown in Figure 5 and Figure 6, the tuned Peng Robinson equation of state predicts the bubble point pressure as a function of temperature accurately for both data sets. For the purposes of this study, therefore, the Peng Robinson equation of state was used to model the behavior of gas mixtures in the absence of DEPG, including during phase change.

PROCESS MODELING

This section presents an overview of the Timmins Process integrated with an IGCC power island such that the relatively high degree of interaction between the various components in the overall system can be appreciated. Details of the design basis and benchmarks for comparison are also

given in this section. Stream level descriptions and process flowsheets for both the Timmins Process and for the IGCC power island are given in the supplementary material that accompanies this paper. All process modeling was undertaken using UniSim Design R400 (Honeywell Inc.).

Overview Of The Timmins Process

A block diagram of the Timmins Process integrated into an IGCC power island is shown in Figure 7. In this Figure, process flows are shown by solid black lines, low pressure (LP), intermediate pressure (IP) and high pressure (HP) steam flows are represented by short-dashed, dotted and long-dashed gray lines and mechanical couplings are shown by gray chain-dashed lines.

The Timmins Process starts after the gasification and hydrogen sulfide removal units and consists of four key steps: acid gas removal, carbon monoxide shift, gas desiccation and carbon dioxide liquefaction and pumping. The sweetened, cooled syngas firstly enters the acid gas removal (AGR) step of the process that uses DEPG as a physical solvent. The first novel feature of the Timmins Process is that the syngas is used as the stripping gas with which to regenerate the rich DEPG solvent. This regeneration process occurs at gasifier pressure, 36 bara, and results in a carbon dioxide rich syngas stream being sent to the carbon monoxide shift unit.

The carbon monoxide shift unit consists of two high temperature shift reactors and a single low temperature shift reactor connected in series. Prior to entering the shift reactors, the carbon dioxide rich syngas is humidified such that the steam to carbon monoxide ratio is at an optimal level for efficient reaction. The carbon monoxide shift reactions are highly exothermic, and the high temperature shift reactor requires a high syngas feed temperature: reaction kinetics for high and low temperature shift catalysts were obtained from the open literature[29]. Two streams of HP boiler feed water (BFW) from the heat recovery steam generator (HRSG) and a stream of IP steam from the steam turbine are exported into the carbon monoxide shift unit for reactor preheating, steam raising and as part of the syngas humidification process respectively. Steam generated as a result of the exotherm within the carbon monoxide shift unit is used to both power an ancillary turbine for mechanical power generation in addition to being used within the syngas humidification process.

After the shifted syngas leaves the carbon monoxide shift unit, gas cooling takes place to allow excess water be removed via condensation. Any remaining water is then removed in a desiccation step to prevent ice formation in the cryogenic unit.

The cryogenic unit partially condenses the carbon dioxide producing a liquid stream that can be pumped to a pressure of 150 bara and a gas stream that contains approximately 36 mol% carbon dioxide, 58 mol % hydrogen with a balance of nitrogen and argon. This step results in removing about 50 % of the total carbon dioxide as a liquid.

The gas stream from the cryogenic unit is sent back to the absorption column in the AGR unit where the DEPG solvent absorbs over 97 % (on a molar basis) of the carbon dioxide. The rich DEPG solvent is then regenerated by the entrant syngas from the gasifier, with the essentially carbon dioxide-free fuel gas stream being sent to the power island for combustion.

The power island is similar to that provided for current state-of-the-art IGCC schemes, where OEMs have developed designs for gas turbines suitable for use with hydrogen-rich fuels[5] such as the GE-7F. The details used in this work are adapted from an existing scheme[30] but key parameters, such as turbine efficiencies, are compared to values reported in the open literature. Additional information is supplied in the supplementary material document that accompanies this paper. The power island consists of four key steps: fuel gas humidification and preheating, combustion and mechanical work generation within twin gas turbines, heat recovery within two parallel HRSGs and mechanical work generation within a single steam turbine. The fuel gas humidification and preheating step requires imports of IP and LP steam from the HRSG such that the composition and temperature conditions can be attained for efficient combustion.

Within the gas turbines, a diluent stream of nitrogen is added such that combustion stoichiometry could be adjusted to its most efficient point. The adiabatic efficiency of the compression and expansion sections of the gas turbine were set at 80.4 % and 87.3 % respectively; these data are consistent with similar data reported in the literature[31], [32]. Exhaust gas from each gas turbine is passed through a HRSG that contains heat exchange elements for the LP, IP and HP BFW circuits, with each circuit having BFW preheaters, boilers and steam superheaters. The IP steam circuit also contains steam reheaters, which are used to superheat IP steam that exits the HP steam turbine such that additional mechanical work can be extracted from the IP and LP stages of the steam turbine. The steam turbine uses a combined steam feed from both HRSGs and consists of a single-shaft machine having HP, IP and LP stages with average adiabatic efficiencies of 86.0 %, 89.8 % and 93.1 %; these data are consistent with similar data reported in the literature[33]. A small amount of IP steam is bled from the turbine for use within both the Timmins Process and the coal gasifier.

Basis For Comparison

In order to compare results from this study to other work in the literature, a decision was taken to model the Timmins Process within an IGCC scheme that had already been characterized. The US DoE baseline studies[5] contain six cases for IGCC power plant, three with carbon capture systems and three without. The key difference between these case studies is the choice of gasifier unit: cases 1 and 2 examine flowsheets with the widely-used General Electric Energy (GEE) gasifier, cases 3 and 4 study flowsheets containing the ConocoPhillips E-Gas™ system that is suited for sub-bituminous coal and cases 5 and 6 investigate flowsheets with the Shell Global Solutions (SGS) gasifier that is capable of gasifying a wide range of fuels. The adaptability of the SGS gasifier was seen to be attractive in terms of developing an IGCC flowsheet that could be deployed widely, hence the flowsheet containing the Timmins Process was based around this unit. For reference, the net power output of case 5 was 629 MWe and case 6 was 497 MWe[5].

A slight complication arises due to the sequence of unit operations within the Timmins Process, since desulferized syngas is required in order to prevent problems within the carbon monoxide shift and cryogenic units. Case 5, which uses a SGS gasifier in a flowsheet without carbon capture, incorporates a Sulfinol™ unit upstream of the gas turbines such that desulferized syngas is burnt. Case 6, having 90 % carbon capture, however, uses a sour shift step upstream of a dual-stage DEPG scrubbing system that removes both hydrogen sulfide and carbon dioxide prior to combustion. This is the preferred process flowsheet arrangement for current IGCC-CCS designs. Due to the use of the syngas as a stripping gas in the AGR unit within the Timmins Process, this dual-stage DEPG system is unsuitable since sulfur-containing compounds would be transferred to the carbon monoxide shift units and would subsequently be present in the cryogenic stage.

The chosen strategy was to use the gasifying and gas clean-up portions of the case 5 flowsheet (up to stream 17 of Exhibit 3-72)[5] to provide syngas to the Timmins Process and then to use the power island and carbon capture specifications from case 6. Case 6 had been designed with a carbon capture level of 90 % (on a mass basis) and contained a power island that had been adapted for use with a high hydrogen fuel, similar to that originating from the Timmins Process.

A key point of note is that the gas turbines within the case 6 power island, consisting of two advanced F-class gas turbines, require a defined fuel gas feed rate. Since the performance of the Timmins Process, which affects the net rate of production of fuel gas, and the power island are tightly interlinked, the modeling was carried out by assuming that the feed into the Timmins

Process was that defined by stream 17 of case 5. If the difference between the rates of fuel gas production and consumption was judged to be "small" (*circa* 5 %), the material and energy flows within the front end of the process (the gasification and gas clean up units within case 5 and the Timmins Process) would be linearly scaled by the capacity difference to obtain an overall energy estimate as opposed to modeling the additional upstream processes at increased capacity. Modeling the gasification and gas clean up units was not part of this study, hence creation of a complete process model at higher capacities than those published would present a significant increase in the number of underlying assumptions due to the proprietary nature of much of the gasifier design data. The incorporation of these assumptions is most likely to introduce a comparable level of uncertainty when compared to a simple scaling, in addition to a significant increase in complexity of the modeling task. The feed composition and conditions (stream 17, case 5)[5] are shown in Table 3.

The initial process model was constructed on the assumption that plant cooling water (CW) was available at 20 °C and that CW heat exchangers were of a conventional shell and tube design operating with a 10 °C minimum approach temperature. Since the refrigeration cycles within the Timmins Process are based upon pre-cooled propane cycles the CW temperature was believed to have a significant effect on refrigeration energy consumption. For this reason, results are also presented for a 15 °C CW temperature with key CW heat exchangers being of a plate-fin design with a minimum approach temperature of 3 °C[34]; this cooling water temperature may be appropriate for some coastal locations in cool climates where direct seawater cooling is used. It may be a challenge sourcing PFHEs suitable for these duties, however there are a number of proprietary designs such as fully welded plate and shell exchangers which can be suitable for hazardous duties and the range of pressures and temperatures which these services experience.

SIMULATION RESULTS AND DISCUSSION

This section highlights key results from the process simulation and presents a comparison between the projected efficiency of the Timmins Process and DoE case 6. The initial simulation of the Timmins Process, termed hereafter as the "base case", assumed that CW was available at 20 °C and that heat exchangers using CW were of a traditional shell and tube design with a minimum temperature approach of 10 °C. A further assumption in this initial case is that all the turbomachinery outside of the power island operated with an isentropic efficiency of 75 %. This

is likely to be significantly lower than commercially-obtainable isentropic efficiencies, but this conservative figure is chosen to offset the effect of other assumptions that have been made to create the process model.

One additional case of the Timmins Process is also presented. This modifies the assumption surrounding the CW temperature and heat exchanger design since the CW temperature directly impacts the pressure ratio within the refrigeration cycles within the Timmins Process and thus influences a significant proportion of the overall flowsheet energy requirement. The modified case assumes that CW is available at 15 °C and that key CW heat exchangers are of a plate fin design with a minimum temperature approach of 3 °C[34].

Performance Of The Timmins Process

The success of the Timmins Process is dependent on the efficient operation of all units within the flowsheet, in particular the AGR unit, the refrigeration cycles, and the HRSG. This is discussed in detail in the supplementary material, and it can be concluded that these key units are operating satisfactorily.

With confirmation of satisfactory HRSG operation, the mechanical energy requirements of the Timmins Process, in the absence of the power island, can be explored. The bar chart shown in Figure 8 illustrates mechanical power use in the Timmins Process as a function of equipment category.

As can be seen from Figure 8, the total net energy consumption of the Timmins Process is 34.2 MW. As expected, the three highest consumers of mechanical energy correspond to the compressors within the two refrigeration cycles and the compressor that recompresses the carbon dioxide rich syngas at the start of the cryogenic unit to account for the accumulated process pressure drop.

The compression ratio within both of the pre-cooled propane refrigeration cycles is entirely dependent of the CW supply since the propane is compressed to the pressure at which CW can change its phase. With a CW temperature of 20 °C and a minimum approach temperature within CW heat exchangers of 10 °C, a propane pressure of 10.8 bara is required. If, however, the CW temperature can be reasonably assumed to be 15 °C and that PFHEs with a minimum approach temperature of 3 °C are used on strategically-chosen cooling duties, then a propane pressure of

only 7.93 bara is needed. The impact on energy use of this change in cooling strategy can be shown in the bar chart in Figure 9.

When the data in Figure 9 and Figure 8 are compared, it can be seen that the energy requirement of the cryogenic refrigeration compressor drops by 17 % and the energy requirement of the refrigeration compressor within the AGR unit drops by 31 %. Both of these figures represent significant energy savings, summing to 6.3 MW; the CoPs of the two refrigeration cycles increase to 4.46 and 5.74 respectively.

In order to quantify the overall efficiency of the power cycle, auxiliary loads for the entire IGCC flowsheet must be calculated and the net power output of the plant calculated. This must then be compared to the higher heating value (HHV) of the fuel supply. Cases 5 and 6 of the US DoE baseline studies[5] present fully quantified auxiliary load summaries in Exhibits 3-75 and 3-89 respectively. Auxiliary load data applicable to processes upstream of the Timmins Process can be taken from DoE case 5, with the data being scaled up by 5.5 % to account for the difference between the optimal fuel gas feed flowrate required by the gas turbines and that produced by the model of the Timmins Process. For ease of comparison, these data have been grouped into categories of coal and slag handling, the air separation unit (ASU), water handling and upstream processes. With regard to the water handling category, BFW and condensate requirements were scaled from the case 5 data with a factor that accounted for the additional BFW flows through the HRSG. DoE case 6 can be used to estimate auxiliary loads downstream of the Timmins Process, in the power island, and hence do not require any scaling. For ease of comparison these data have been grouped into the category of "other losses".

In terms of the energy supplied from the fuel, it is assumed that Illinois number 6 coal is used with a HHV of 27,135 kJ/kg; this is the same fuel supply as DoE case 5[5]. The rate of energy input to the IGCC process is assumed to be that of DoE case 5 scaled up by 5.5 %, which corresponds to 1.57 GW.

A comparison between the energy requirements for DoE cases 5 and 6 and the two variants of the Timmins Process that have been presented is shown in the bar charts in Figure 10 and Figure 11; Figure 10 shows a breakdown of the auxiliary load data and Figure 11 illustrates the differences between gross and net power generation.

When the four data sets are compared, it can be seen that both variants of the Timmins Process compare very favorably with respect to case 6, which is the IGCC case with 90 % carbon capture.

It must be noted when comparing these data that the Timmins Process was converged to a carbon capture level of 91.8 %, hence there is an additional margin for error built into these results to account for assumptions made during the modeling process. A plot that gives a comparison of the overall percentage efficiency of the four processes that have been described, based on the HHV of the fuel, is given in Figure 12.

The data shown in Figure 12 illustrates that the Timmins Process can integrated within an IGCC power plant with net plant HHV efficiencies between 33.8 % and 34.3 %, depending on the nature of the CW supply and circuit design. It is very possible that the attainable efficiency is higher than these values due to the conservative approach that has been taken for this study. These efficiencies correspond to specific primary energy consumption for CO_2 avoided (SPECCA) values[35] of 2.95 and 2.75 respectively; more information on this calculation is provided in the supplementary material. These results compare very favorably against the DoE IGCC studies, where the net plant HHV efficiencies range between 32.6 % (case 2) and 31.0 % (case 4); case 6 had a net plant HHV efficiency of 31.2 %. These higher efficiencies are due to the Timmins Process' unique combination of using high pressure syngas to regenerate the DEPG solvent, its use of cryogenic pumping to pressurize the CO_2 to supercritical state and the presence of a high-performing pre-cooled propane refrigeration cycle to liquefy the CO_2.

This study contains a number of approximations and assumptions, all of which have been outlined in the appropriate parts of this paper, which may impact the quoted results to a limited extent. The largest degrees of uncertainty surround the accuracy of the thermodynamics of the interaction between DEPG and the components within syngas, the transition between different thermodynamic models across the flowsheet and the linear scaling to allow the turbine data from DoE case 6 to be used with the gasification front-end of DoE case 5. Thermodynamic parameters describing these interactions have been regressed to the best possible extent using data in the open literature, but further investigation with specialist, commercially-available, models is recommended. The margin between IGCC with an embedded Timmins Process and DoE case 6 equates to 41.4 MW of additional power: this is approximately 2.7 times greater than the combined energy requirement of all gasification and gas-clean up processes in Case 5, excluding the operation of the air separation unit. It is unlikely that the linear scaling of energy requirements from Case 5 by a factor of 1.055 would result in a 2.7-fold increase in energy requirements of these

processes. A reasonable degree of confidence can therefore be had about the favorable net plant HHV efficiencies and SPECCA values for IGCC with embedded Timmins.

The impact of other assumptions within this study has also attempted to be reduced by increasing the extent of carbon capture of the Timmins Process to 91.8 % on a mass basis, by comparing these results to the DoE case studies that are valid for 90.0 % carbon capture, and by using adiabatic efficiencies of only 75 % for all items of turbomachinery outside the power island. More detailed analysis of the interaction between the power island and the Timmins Process is recommended, in particular the operation of the HRSG, as is examination of the effect of thermodynamic transitions across the flowsheet. With these caveats stated, it can be concluded from the results of this study that the Timmins Process is a potentially very promising technology that could pave the way for a new generation of high efficiency IGCC power plants.

CONCLUSIONS

This initial study has shown that the Timmins Process, a novel pre-combustion carbon capture process, is capable of being incorporated within an IGCC flowsheet resulting in a power plant with net efficiencies between 33.8 % and 34.3 %, measured at 91.8 % (mass basis) carbon capture and referenced against the HHV of the fuel. The exact efficiency obtained depends on the flowsheet configuration and the CW conditions. These efficiency figures are also influenced by a number of assumptions that have been described in this paper, and further validation work is recommended. This compares favorably with the US DoE studies, where the most efficient IGCC flowsheet had a net plant HHV efficiency of 32.6 %.

The Timmins Process contains unit operations that have been industrially-proven over a long period of time; the novelty within this process is the sequence with which they are used. The Timmins Process, therefore, should present relatively low technical risk to potential investors.

Two key parameters that influence the overall efficiency of the Timmins Process are the temperature of the cooling water that is used and the isentropic efficiency of the turbomachinery. Scope for further optimization exists surrounding these two parameters.

This study has also developed and presented a regressed set of Henry's law parameters that describe the interaction of DEPG with components typically found in syngas.

ACKNOWLEDGEMENTS

The authors gratefully acknowledge the UK Technology Strategy Board for funding *via* strand two of the Carbon Abatement Technology call, 2011. Honeywell Inc. is gratefully acknowledged for research use of UniSim R400 as part of its Universities Program. Useful discussions with Dr A.R. Williams regarding gas solubilities in DEPG is also gratefully acknowledged.

NOMENCLATURE

Roman Letters

A	Binary interaction parameter	-
B	Binary interaction parameter	K
C	Binary interaction parameter	-
D	Binary interaction parameter	K^{-1}
H_{ij}	Henry's coefficient	kPa
K_{ij}	Mixture correction term	-
P	Pressure	kPa
T	Temperature	K
x	Liquid phase mole fraction	-
y	Gas phase mole fraction	-

Greek letters

α_{ij}	K_{ij} interaction parameter	-
β_{ij}	K_{ij} interaction parameter	K^{-1}
γ_{ij}	K_{ij} interaction parameter	K^{-2}
δ_{ij}	K_{ij} interaction parameter	-
ϵ_{ij}	K_{ij} interaction parameter	K

Abbreviations

AGR	Acid gas removal	HP	High pressure
ASME	American Society of Mechanical Engineers	HRSG	Heat recovery steam generator
BFW	Boiler feed water	HTS	High temperature CO shift
CCS	Carbon capture and storage	IGCC	Integrated gasifier combined cycle
CoP	Coefficient of performance	IP	Intermediate pressure
CW	Cooling water	LHV	Lower heating value
DEPG	Dimethyl ethers of polyethylene glycol	LP	Low pressure
		LTS	Low temperature CO shift
DoE	US Department of Energy	NRTL	Non-random two liquid
GEE	General Electric Energy	PFHE	Plate and fin heat exchanger
HHV	Higher heating value	SGS	Shell Global Solutions

REFERENCES

[1] T. Kuramochi, A. Ramírez, W. Turkenburg, A. Faaij, *Prog. Energy Combust. Sci.*, **2012**, *38*, 87.

[2] A. C. Todd, B. Tohidi, A. Fredheim, G. Maitland, P. Fennell, S. Brandani, J. Gibbins, G. Stevens, J. C. M. Pires, F. G. Martins, M. C. M. Alvim-Ferraz, M. Simões, *Chem. Eng. Res. Des.*, **2011**, *89*, 1446.

[3] IEA, *Key World Energy Statistics 2011*, OECD Publishing, Paris **2011**.

[4] A. Padurean, C.-C. Cormos, P.-S. Agachi, *Int. J. Greenh. Gas Control*, **2012**, *7*, 1.

[5] J. Black, *Cost and Performance Baseline for Fossil Energy Plants Volume 1: Bituminous Coal and Natural Gas to Electricity*, 2nd edition, DOE/NETL - 2010/1397 **2010**.

[6] J. Gale, H. Herzog, J. Braitsch, K. E. Zanganeh, A. Shafeen, C. Salvador, *Energy Procedia*, **2009**, *1*, 247.

[7] R. Boehm, J. T. Kim, S. Riffat, W. Chun, A. A. Olajire, *Energy*, **2010**, *35*, 2610.

[8] C. Kunze, H. Spliethoff, *Appl. Energy*, **2012**, *94*, 109.

[9] A. L. Kohl, R. Nielsen, *Gas Purification*, 5th edition, Gulf Professional Publishing, Houston **1997**.

[10] C. Higman, M. van der Burgt, *Gasification*, 2nd edition, Elsevier Ltd, Burlington **2008**.

[11] C.-C. Cormos, *Int. J. Hydrogen Energy*, **2009**, *34*, 6065.

[12] R. D. Doctor, J. C. Molburg, P. Thimmapuram, G. F. Berry, C. D. Livengood, R. A. Johnson, *Energy Convers. Manag.*, **1993**, *34*, 1113.

[13] R. W. Bucklin, R. L. Schendel, *Energy Prog.*, **1984**, *4*.

[14] WO 2009109737, (**2009**), invs.: C. Timmins.

[15] C. Timmins, C. Hodrien, "A “step-change” low-energy pre-combustion CO2 capture process", *Gasification 2010*, IChemE, Amsterdam, **2010**.

[16] C. Hodrien, B. Hallmark, *Mod. Power Syst.*, **2013**, *33*, 16.

[17] Y. Xu, R. P. Schutte, L. G. Hepler, *Can. J. Chem. Eng.*, **1992**, *70*, 569.

[18] B. Burr, L. Lyddon, "A Comparison of Physical Solvents for Acid Gas Removal", *87th Annual GPA Convention*, GPA Midstreasm Association, Grapevine, TX, **2008**.

[19] Honeywell, *UniSim Design - Simulation Basis Reference Guide*, **2010**.

[20] R. P. Field, R. Brasington, *Ind. Eng. Chem. Res.*, **2011**, *50*, 11306.

[21] J. Gross, G. Sadowski, *Ind. Eng. Chem. Res.*, **2001**, *40*, 1244.

[22] H. Renon, J. M. Prausnitz, *AIChE J.*, **1968**, *14*, 135.

[23] D. B. Robinson, D.-Y. Peng, S. Y.-K. Chung, *Fluid Phase Equilib.*, **1985**, *24*, 25.

[24] A. R. Williams, *Private Communication*, **2014**.

[25] W. Linke, *Solubilities Volume 1; inorganic and metal-organic compounds*, 4th edition, D. Van Nostrand Inc., Princeton **1958**.

[26] J. Timmermans, *The Physico-Chemical Constants of Binary Systems in Concentrated Solutions Volume 4.*, Interscience Publishers Inc., New York **1960**.

[27] Honeywell, *UniSim Thermo Reference Guide*, **2010**.

[28] T. O. Kvålseth, *Am. Stat.*, **1985**, *39*, 279.

[29] H. Rase, J. Holmes, *Chemical reactor design for process plants*, John Wiley & Sons, New York **1977**.

[30] I. Salmon, *Private communication*, **2012**.

[31] WO2014055307, (**2013**), invs.: M. Coney.

[32] E. Catalanotti, M. Pourkashanian, *Carbon Capture: A Technology Assessment Evaluation of Performance and Cost of Combustion Based Power Plants with CO 2 Capture in the UK*, The Centre for Low Carbon Futures, Leeds **2012**.

[33] R. Sanjay, O. Singh, "Thermodynamic Evaluation of Advanced Combined Cycle Burning Hydrogen", *Proc. NHA Annual Hydrogen Conference*, National Hydrogen Association, Sacramento, CA, USA, **2008**.

[34] K. Thulukkanam, *Heat Exchanger Design Handbook*, CRC Press, Boca Raton **2013**.

[35] R. Anantharaman, O. Bolland, N. Booth, E. van Dorst, C. Ekstrom, E. Sanchez Fernandes, F. Franco, E. Macchi, G. Manzolini, D. Nikolic, A. Pfeffer, M. Prins, S. Revani, L. Robinson, *European best practice guidelines for assessment of CO2 capture technologies*, European Benchmraking Task Force, Milan **2011**.

LIST OF FIGURES

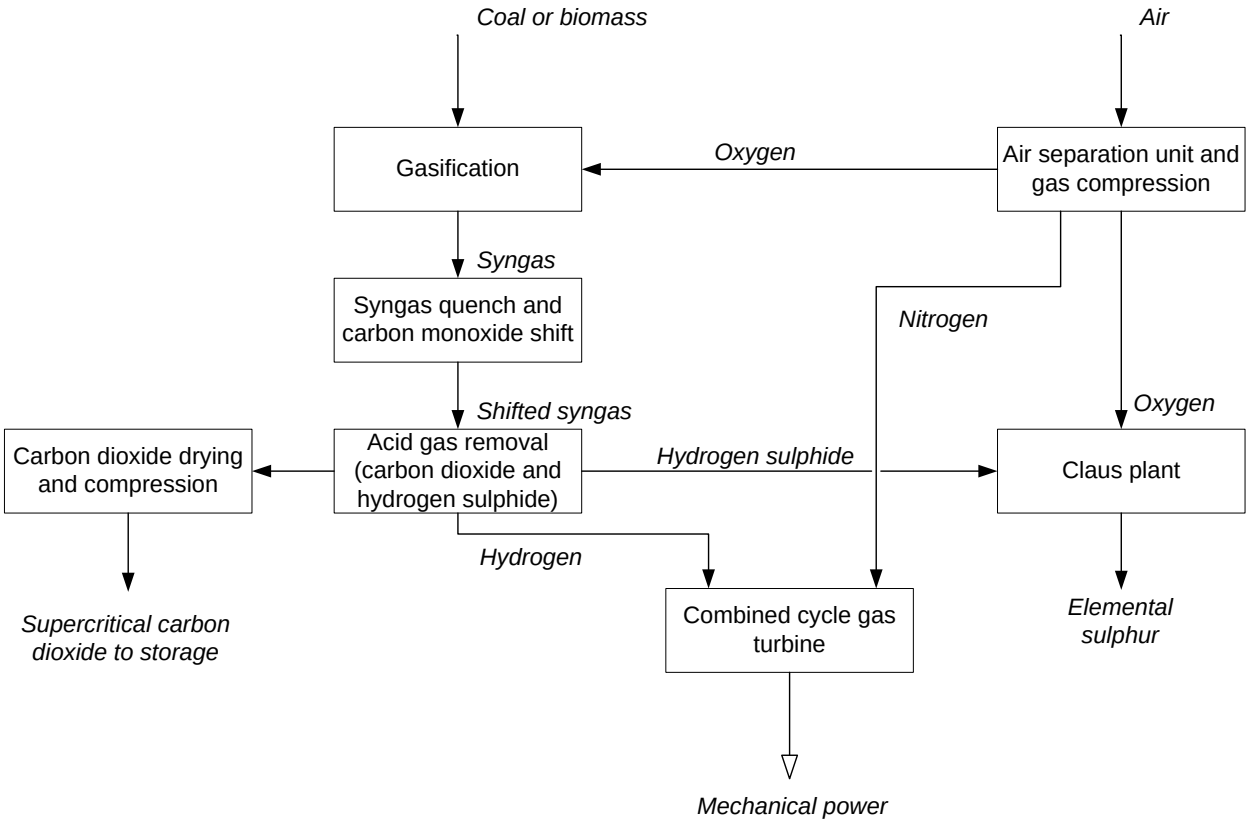

Figure 1. Block diagram of a typical IGCC scheme with carbon capture (adapted from Cormos[11])

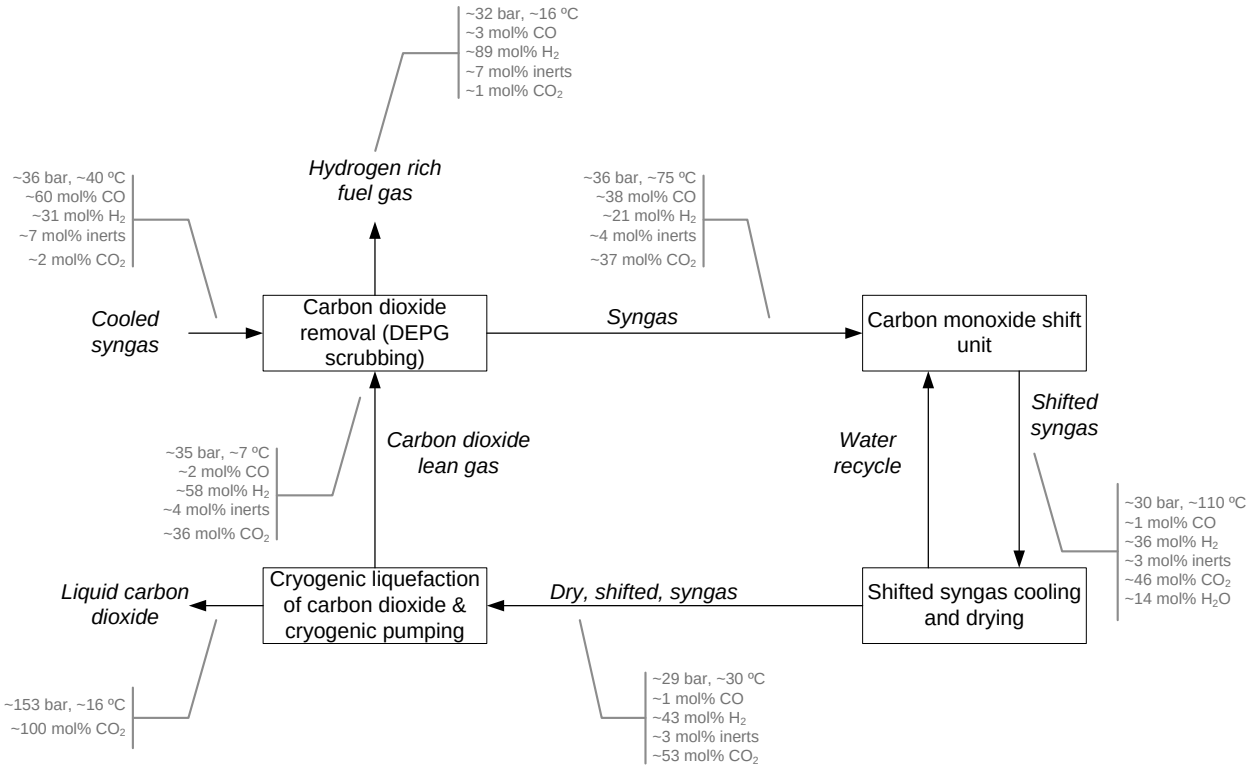

Figure 2. Simplified block diagram of the Timmins Process (adapted from Timmins and Hodrien[15])

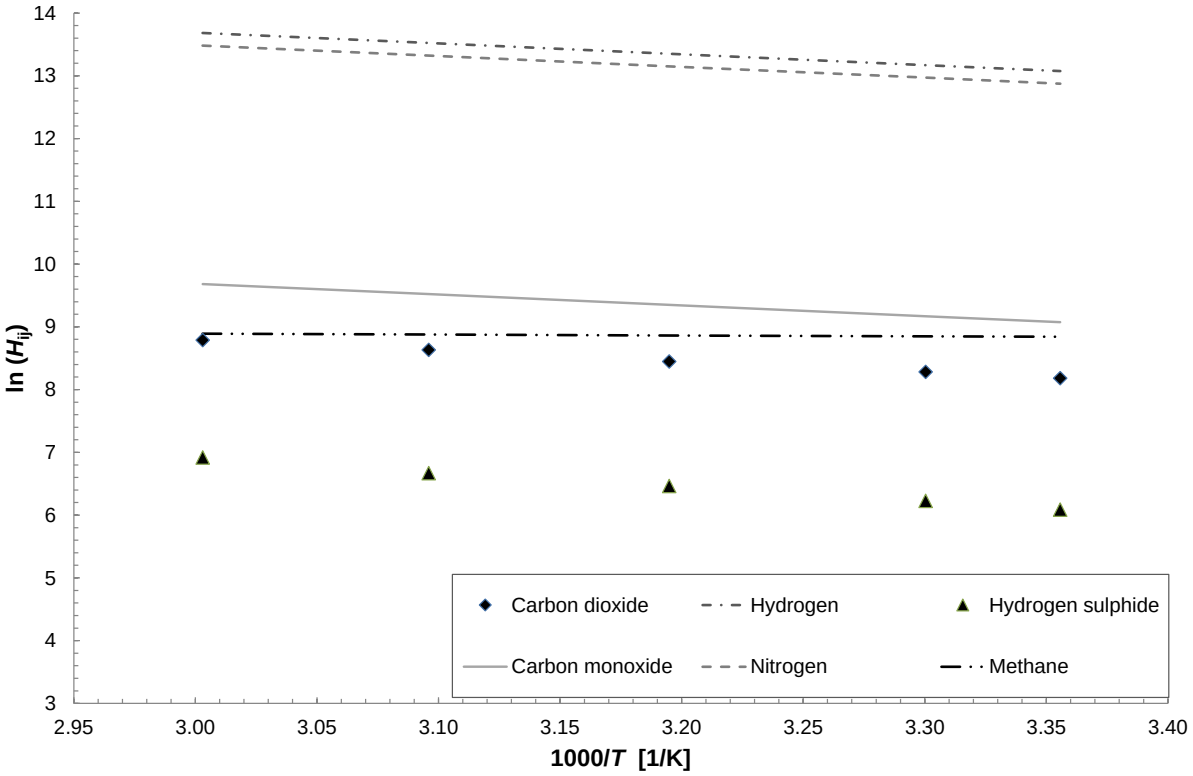

Figure 3. Plot of the natural logarithm of Henry's constant as a function of reciprocal temperature. Individual data points correspond to experimental data for carbon dioxide and hydrogen sulfide[17] and solid lines represent regressed data based on solubility ratios at 25 °C and 1 atmosphere[18].

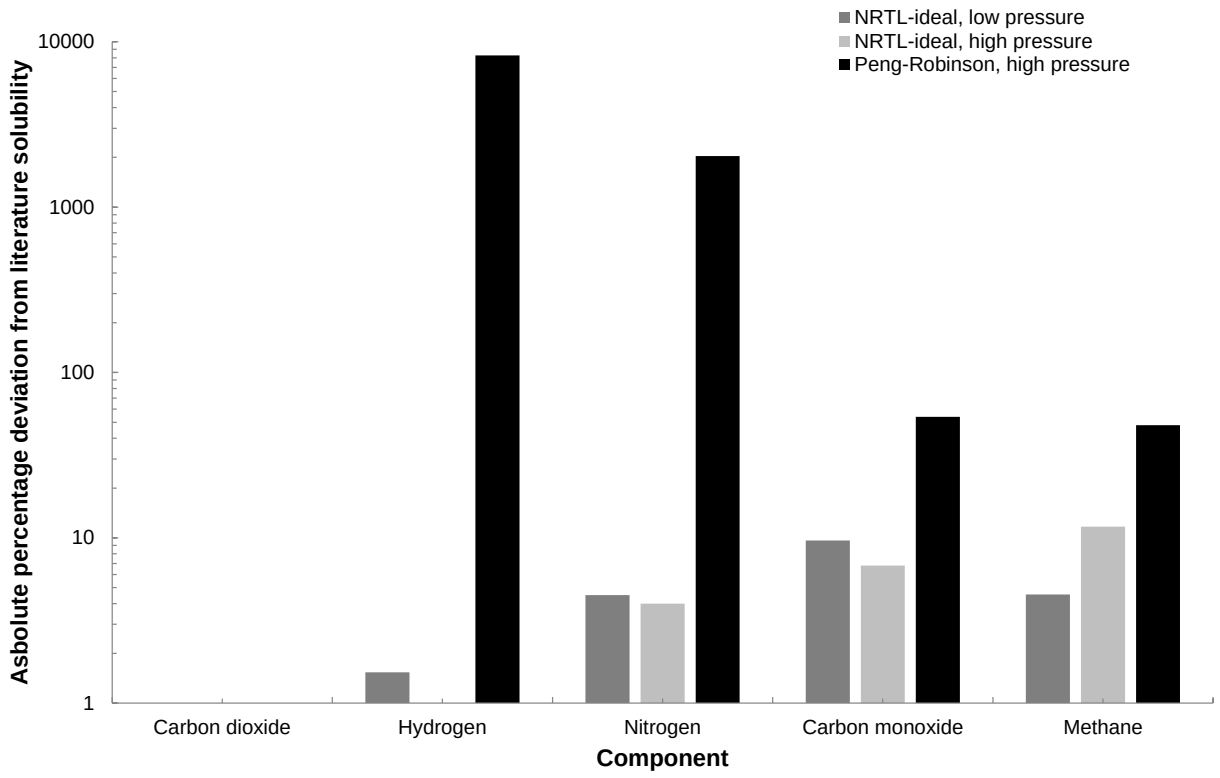

Figure 4. Plot of the relative solubility of syngas components compared to literature values predicted by different thermodynamics models.

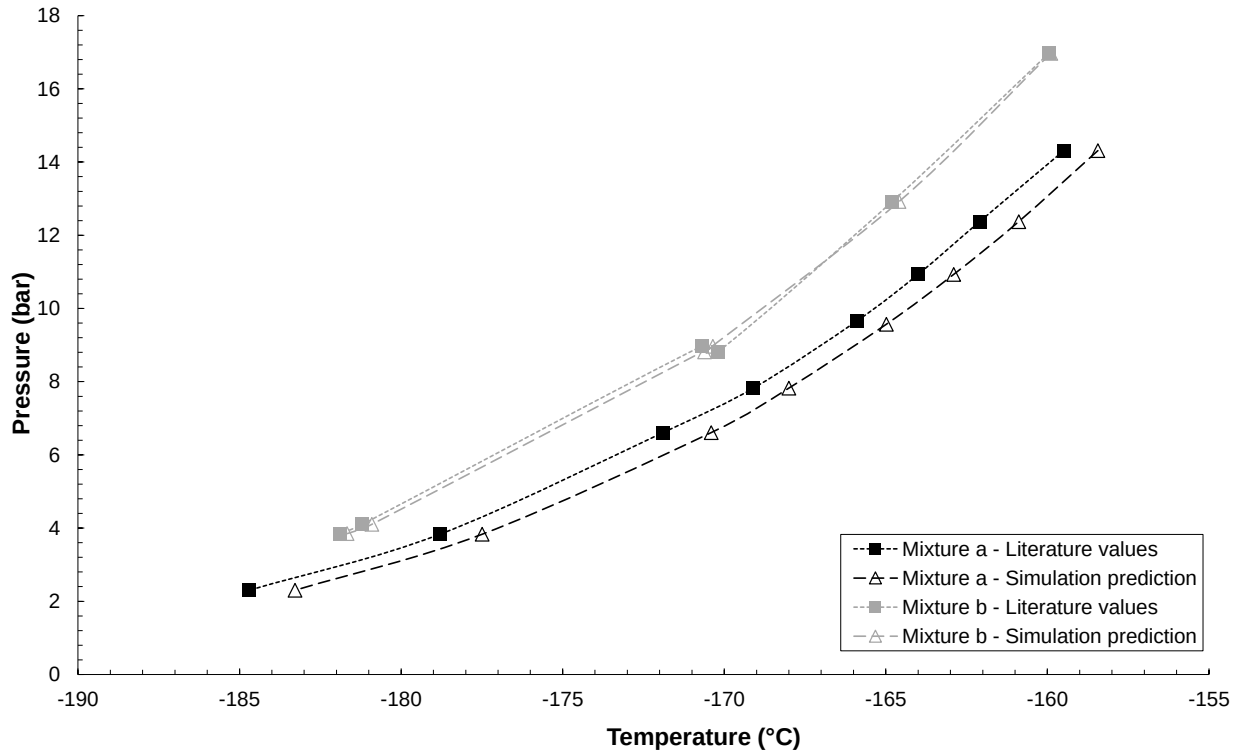

Figure 5. Plot of the bubble point pressure of mixtures of nitrogen and carbon monoxide as a function of temperature. Closed symbols represent literature values[25], open symbols represent predictions by the Peng Robinson equation of state. Mixture (a): 59.7 mol% carbon monoxide, balance nitrogen. Mixture (b): 16 mol% carbon monoxide, balance nitrogen. Lines between data points for visual guidance only.

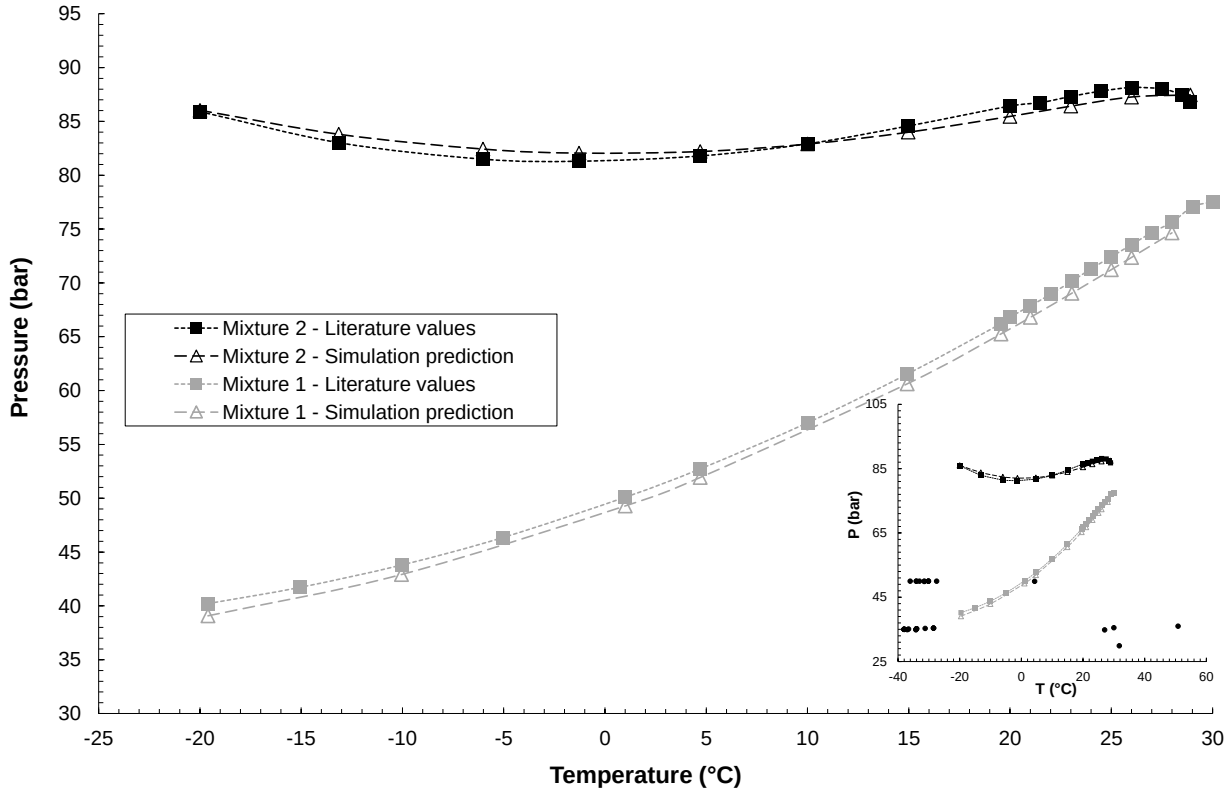

Figure 6. Plot of the bubble point pressure of mixtures of hydrogen, carbon dioxide and carbon monoxide as a function of temperature. Closed symbols represent literature values[26], open symbols represent predictions by the Peng Robinson equation of state. Mixture (1): 0.07 mol% carbon monoxide, 0.97 mol% hydrogen, balance carbon dioxide. Mixture (2): 0.25 mol% carbon monoxide, 3.2 mol% hydrogen, balance carbon dioxide. Lines between data points for visual guidance only. Inset plot illustrates cryogenic unit conditions within the Timmins process.

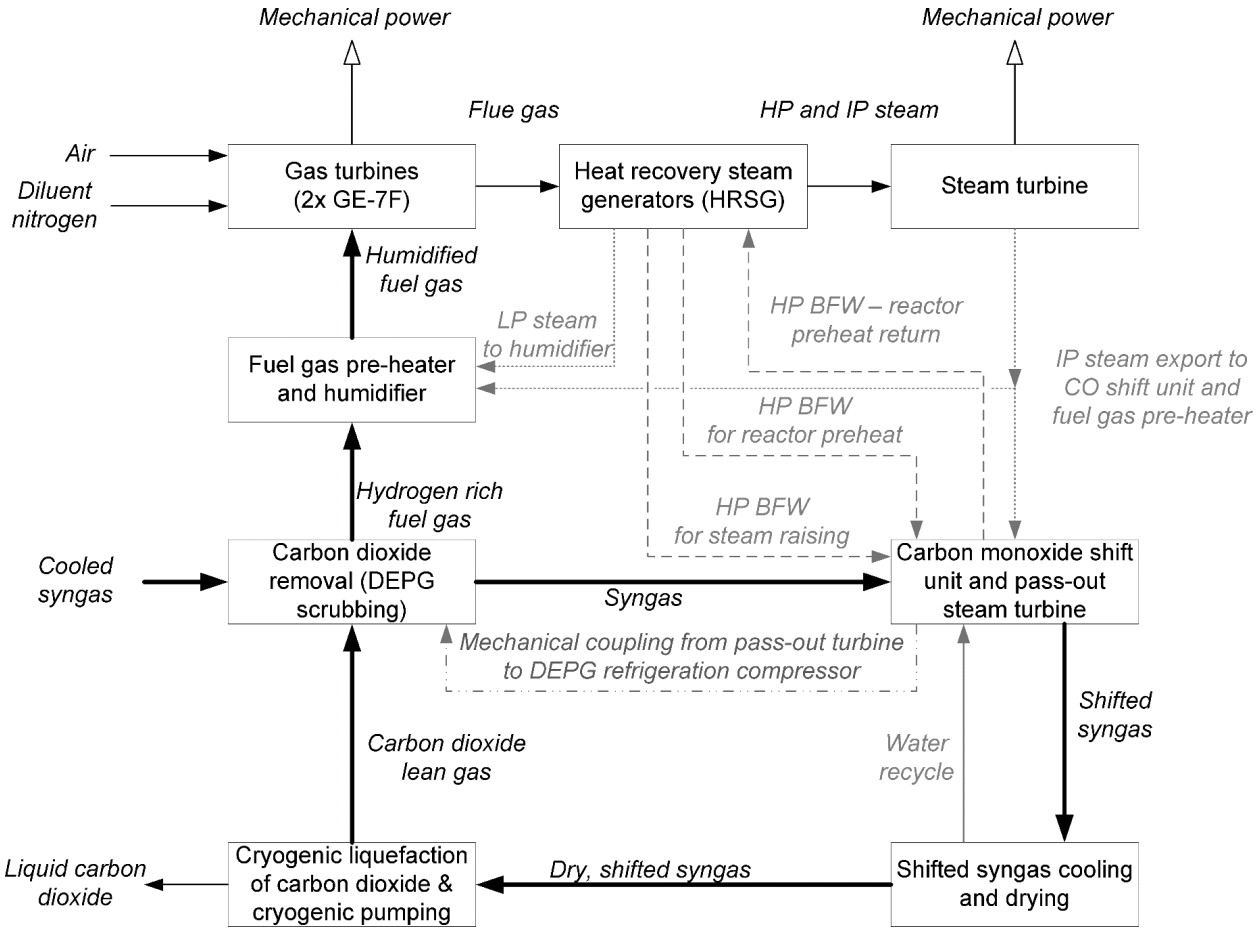

Figure 7. Block diagram of Timmins integrated with an IGCC power island.

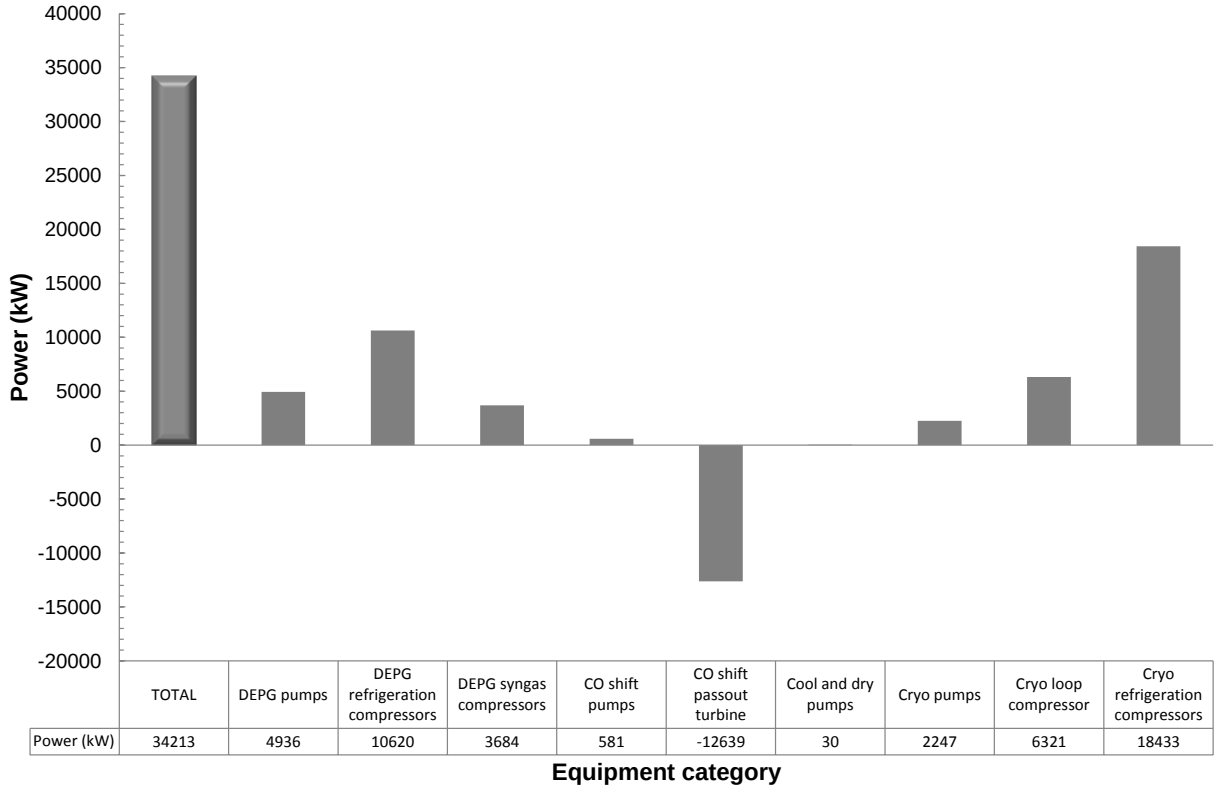

	TOTAL	DEPG pumps	DEPG refrigeration compressors	DEPG syngas compressors	CO shift pumps	CO shift passout turbine	Cool and dry pumps	Cryo pumps	Cryo loop compressor	Cryo refrigeration compressors
Power (kW)	34213	4936	10620	3684	581	-12639	30	2247	6321	18433

Figure 8. Plot of mechanical energy use as a function of equipment category for the "base case" of the Timmins Process.

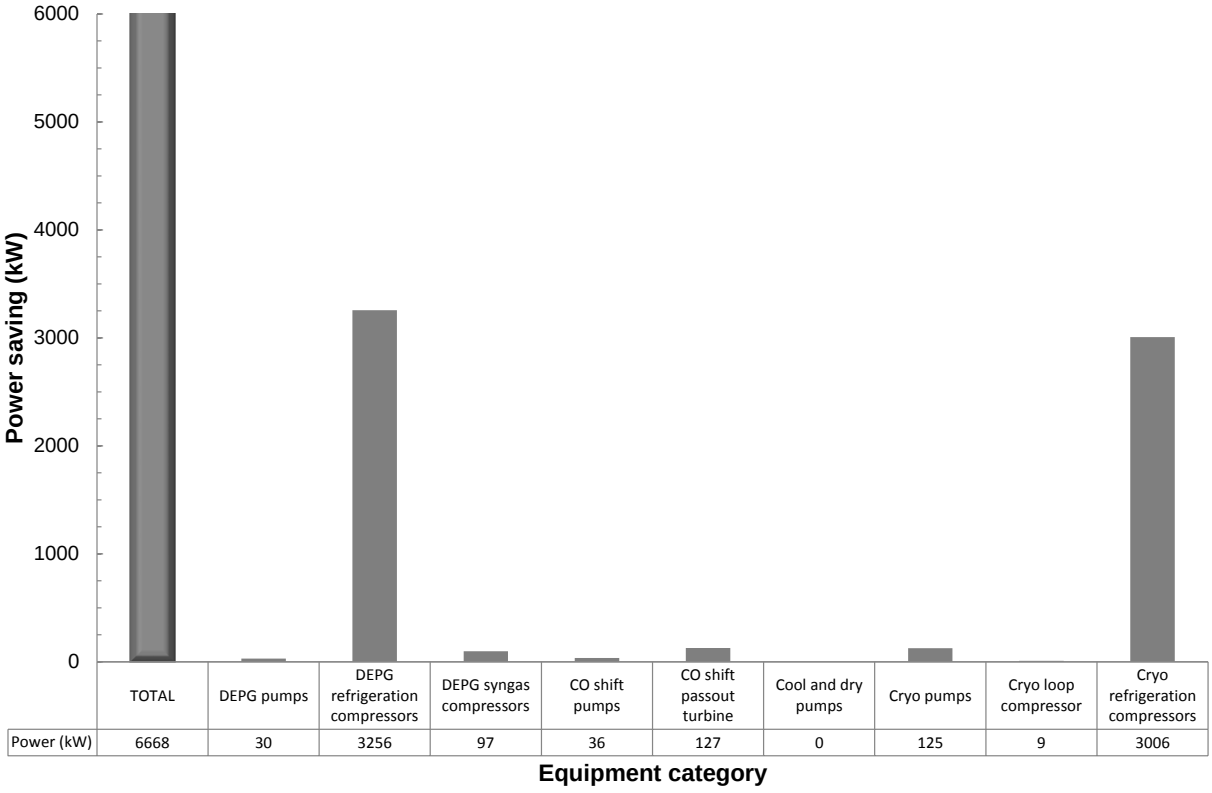

Figure 9. Plot of the power savings obtained with a CW temperature of 15 °C using PFHEs as a function of equipment category.

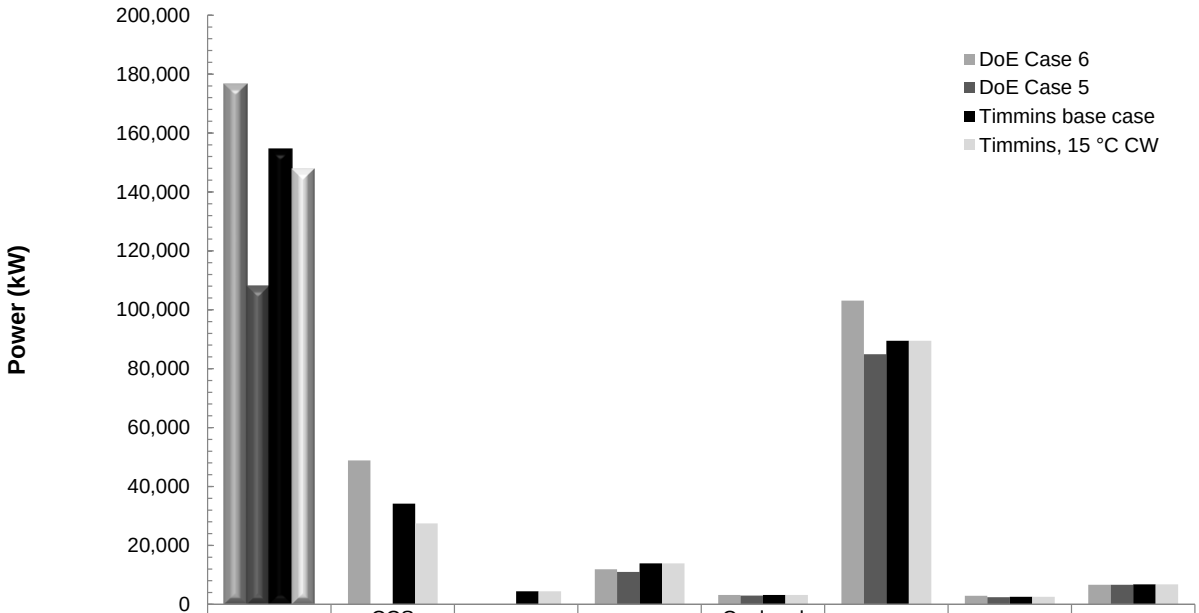

	TOTAL (kW)	CCS system less net energy export (kW)	CCS additional energy (kW)	Water handling (kW)	Coal and slag handling (kW)	ASU (kW)	Upstream processes (kW)	Other losses (kW)
DoE Case 6	176,540	48,860	0	11,890	3,180	103,110	2,870	6,630
DoE Case 5	108,020	0	0	11,030	3,000	84,930	2,440	6,620
Timmins base case	154,547	34,183	4444	13,915	3,160	89,466	2,570	6,809
Timmins, 15 °C CW	147,869	27,505	4444	13,915	3,160	89,466	2,570	6,809

Figure 10. Bar chart showing the total energy requirement and a breakdown of the auxiliary load data for DoE cases 5 and 6 along with the base case Timmins Process and the Timmins Process with 15 °C CW.

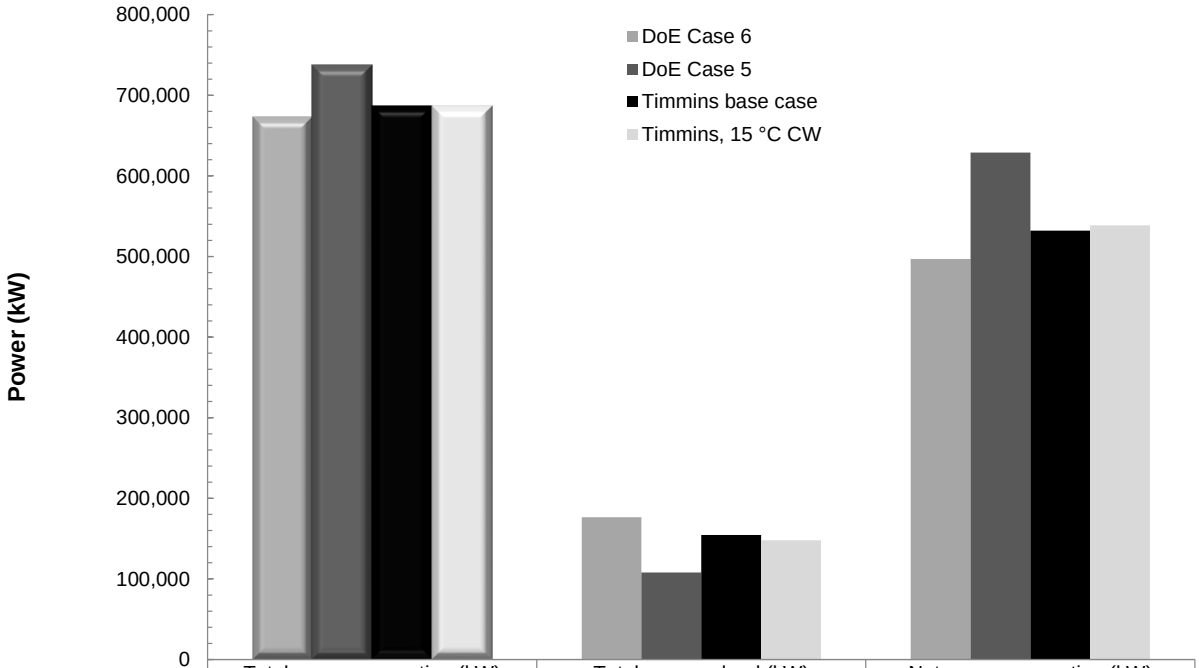

	Total power generation (kW)	Total process load (kW)	Net power generation (kW)
DoE Case 6	673,400	176,540	496,860
DoE Case 5	737,000	108,020	628,980
Timmins base case	686,600	154,547	532,053
Timmins, 15 °C CW	686,600	147,869	538,731

Figure 11. Bar chart showing the gross power generation, total process load and net power generation of DoE cases 5 and 6 along with the base case Timmins Process and the Timmins Process with 15 °C CW.

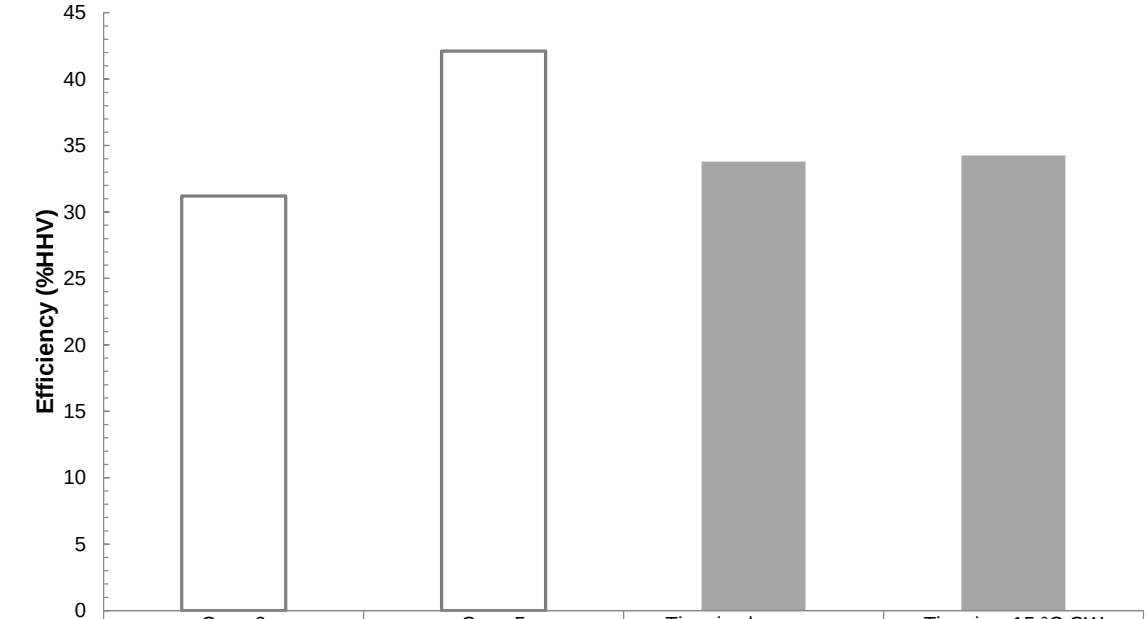

Figure 12. Bar chart showing the overall plant efficiency of DoE cases 5 and 6 along with the base case Timmins Process and the Timmins Process with 15 °C CW. Solid gray bars indicate the Timmins Process model having turbomachinery isentropic efficiencies set to 75 % and black bars indicate an elevated isentropic efficiency of either 80 % or 86 % depending on the unit operation.

LIST OF TABLES

Table 1. Key process modeling assumptions

	Nature of assumption	Key references	Likely impact on process model
1	Thermodynamics of CO_2, H_2, CO and N_2 interacting with DEPG suitably described by NRTL (liquid phase) and ideal gas (vapor phase.	**Solubility data:** Xu *et al.*[17] Burr & Lyddon[18] **Methdology:** Field & Brasington[20] **Validation data:** Burr & Lyddon[18] Williams[24]	Key assumption and further discussion given in main text of article. Model converged to 91.8% capture (on a mass basis) to give margin for uncertainty.
2	Thermodynamics of liquefaction of CO_2 / CO / H_2 gas mixtures described by Peng-Robinson equation of state.	**Bubble point data:** Linke[25] Timmermans[26]	CO_2 bubble point behavior tuned against experimental data such that coefficient of determination (R^2) > 0.9. More discussion in main text of article. High degree of confidence in simulation prediction.
3	CO shift reaction kinetics for high temperature and low temperature shift catalysts.	**Kinetic data:** Rase [27]	Established literature data. High degree of confidence in simulation prediction.
4	Adiabatic efficiency of GE-7F compression and expansion sub-units set to 80.4 % and 87.3 %	**GE-7F data:** Catalanotti[30] Coney[29]	Overall GE-7F adiabatic efficiency stated to be 84 %[30]. GE-7F compressor polytropic efficiency stated to be ~88 %[29]. Efficiency figures used in this study close to reported values – high degree of confidence in simulation prediction.
5	Adiabatic efficiency of HP, IP and LP units of steam turbine set to 86.0 %, 89.8 % and 93.1 %.	**Steam turbine data:** Sanjay & Singh[31]	Sanjay and Singh suggest isentropic efficiencies from HP to LP ranging from 88 % to 92 %. Adiabatic efficiencies used represent polytropic efficiencies 86 % to 92 %. Efficiency figures used in this study close to reported values – high degree of confidence in simulation prediction.
6	HRSG pinch temperature set to 6 °C	**HRSG data:** Kehlhofer *et al.*[33] Ganapathy[34]	Accepted wisdom that 10 °F pinch termperature is attainable when using finned evaporator tubes. Final HRSG pinch temperature of 7.2 °C within this limit – high confidence in simulation prediction of heat recovery system.
7	Upscaling DoE case 5 and Timmins process capacities by 5 % to allow hydrogen production process to supply feed required by GE-7F turbines in DoE case 6	**Case 5 and 6 data:** Black[5]	Linear scaling subject to a degree of uncertainty, but likely to have less uncertainty than modelling gasification and air separation process. Medium-high confidence since an increase in process scale of 1.05 would have to result in an increase in energy requirements of 2.70 in order to reduce efficiency of IGCC-Timmins to that of DoE case 6.

Table 2. Binary interaction parameters for carbon dioxide, hydrogen sulfide, hydrogen, carbon monoxide, nitrogen and methane.

	Carbon dioxide	Hydrogen sulphide	Hydrogen	Carbon monoxide	Nitrogen	Methane
Intercept, *A*	13.957	13.84	18.85	14.85	18.65	9.31
Gradient, *B* (K)	-1721.1	-2309.5	-1721.1	-1721.1	-1721.1	-139.9

Table 3. Syngas composition and conditions (taken from stream 17 of DoE case 5)[5]

Pressure	36.5	bar absolute
Temperature	44.4	°C
Flow rate	16770	kmol/hr
Component	Composition (mol %)	
Water	0.13	
Carbon dioxide	1.58	
Hydrogen sulphide	0.00	
Hydrogen	31.42	
Carbon monoxide	59.80	
Nitrogen	6.01	
Argon	1.00	
Methane	0.06	

The Timmins Process – a novel approach for low energy pre-combustion carbon capture in IGCC flowsheets.

SUPPLEMENTARY MATERIAL

This document describes in detail the process flowsheets that were modeled to quantify the overall energy use of the Timmins Process. Process flow diagrams and detailed descriptions are given for each of the four key units within the Timmins Process and for the three units that comprise the power generation island. Also included within this document is a detailed appraisal of the operation of acid gas removal unit and refrigeration cycles within the Timmins Process and of the heat recovery steam generator within the power generation island.

MODELING THE TIMMINS PROCESS

Acid Gas Removal (AGR) Unit

The physical solvent that was used in the AGR unit was DEPG, with chemical formula $CH_3O(C_2H_4O)_nCH_3$ where n ranges from 2 to 9[1]. In this model, DEPG is represented by the "Selexol" component from the databank supplied with UniSim Design R400, with an average molecular weight of 290 corresponding to n = 5.54. The thermodynamic basis within UniSim was set to NRTL for the liquid phase and ideal gas for the vapor phase, with the binary interaction parameters shown in Table 1 of the main paper being used to describe the interactions between DEPG and the key components within syngas. A flowsheet for the AGR unit is shown in Figure S1.

The syngas from Sulfinol unit (GAS-102) is fed directly into the bottom of the stripper (C-101, 14 theoretical stages), contacting rich solvent (SEL-102b) in a counter current fashion resulting in solvent regeneration. The carbon dioxide rich gas (GAS-103) leaves the column, is combined with a gas recycle (GAS-108) and sent to the carbon monoxide shift unit (GAS-109). During the regeneration process, DEPG undesirably absorbs an amount of carbon monoxide. The regenerated solvent (SEL-103) is, therefore, reduced in pressure to 5 bara and the resulting gas stream (GAS-104) is compressed back to process pressure by a multiple stage intercooled centrifugal compressor (K-101, K-105) with an assumed isentropic efficiency of 75 %.

The DEPG is pumped back to 34.8 bara (P-110) prior to being cooled in a feed-effluent heat exchanger (E-104), a heat exchanger associated with heat recovery (E-109) and a plate fin heat exchanger (PFHE, E-111) associated with a refrigeration cycle. The DEPG enters the scrubbing column (C-102, 21 theoretical stages) at -6.5 °C. Cold DEPG contacts carbon dioxide rich fuel gas from the cryogenic unit (GAS-443) in C-102 and removes over 97 mol% of the carbon dioxide. The energy efficiency of the carbon dioxide removal process within C-102 is enhanced by taking a DEPG side draw from stage 16 (where stage 1 is designated to be the top of the column), which is at 12 °C, chilling it to 6 °C, and returning it to stage 12. The molar flow of the side draw (SEL-110) was optimized to be 12000 kmol/hr, roughly 52 % of the total DEPG flow.

The rich DEPG (SEL-100) leaves C-102 at about 13 °C and is warmed by E-104 and E-217 to approximately 84 °C prior to reentering C-101; the heat source used in E-217 results from heat integration with carbon monoxide shift unit. Minimum temperature approaches of 10 °C were assumed in heat exchangers E-104, E-109 and E-217.

DEPG cooling was provided by a pre-cooled propane cycle that used CW to drive the phase change of the propane from gas to liquid (using E-113). The temperature of the liquid propane (PRO-102) was assumed to be 30 °C, hence requiring a pressure of 11.4 bara; this temperature was dropped to 25.6 °C by heat recovery with the syngas leaving C-102 in PFHE E-114. The propane flow was split into two circuits, PRO-103 and PRO-105, with PRO-103 being let down in pressure to 3.50 bara and PRO-105 being let down to 5.00 bara. The 3.50 bar propane stream, at -9.5 °C, contacted the lean DEPG in PFHE E-111, cooling the DEPG to -6 °C, and the 5.00 bara propane stream contacted the DEPG side draw in PFHE, E-118. Minimum temperature approaches of 3 °C were assumed in all PFHE units[2]. The two compressors within the refrigeration cycle, K-112 and K-117, were assumed to operate at an isentropic efficiency of 75 %.

Carbon Monoxide Shift Unit

The carbon monoxide shift unit converts carbon monoxide and steam to hydrogen and carbon dioxide, according to the equilibrium reaction shown in Reaction [a].

$$CO + H_2O \rightleftharpoons H_2 + CO_2$$

[a]

In industrial applications, specialist catalyst vendors would be contacted to confirm kinetic performance of the sweet shift catalyst. However due to the nature of the study, and the

preference to use open source literature where possible, the following approach was taken. Reaction kinetics were found in the open literature for a chromia-promoted iron oxide high temperature shift (HTS) catalyst and a copper-zinc oxide low temperature shift (LTS) catalyst[3]. The rate expression is given as:

$$(-r_{\mathrm{CO}}) = \frac{\varphi k \left(y_{\mathrm{CO}} y_{\mathrm{H_2O}} - \frac{y_{\mathrm{CO_2}} y_{\mathrm{H_2}}}{K} \right)}{379 \rho_b} \tag{1}$$

In Equation (1), the rate, $(-r_{\mathrm{CO}})$, is in terms of pound-moles of carbon monoxide converted per pound of catalyst per hour, y_i is the gas phase mole fraction of component i, ρ_b is the catalyst bulk density in pounds per cubic feet, T is the temperature in Rankine, k is the rate constant, K is the equilibrium constant and φ is the activity factor. The last three parameters in this list are dependent on the catalyst type and on the reactor conditions. Expressions for these parameters are given in Table S1; in this Table temperatures are again measured in Rankine and pressures, P, are measured in atmospheres.

The thermodynamic behavior of gas mixtures in this unit is modeled using the Peng Robinson equation of state except for heat exchange streams that consist of entirely steam or water. These streams were modeled using the ASME steam thermodynamic package within UniSim Design[4]. Transitions in the thermodynamic model between the AGR unit and the carbon monoxide shift unit were handled by preserving the temperature and pressure of a stream across the transition. A flowsheet for the carbon monoxide shift unit is shown in Figure S2.

The carbon dioxide rich syngas leaving the AGR unit (GAS-109) first passes in a counter current fashion through two packed columns, C-200 (10 theoretical stages) and C-202 (10 theoretical stages) where it contacts hot water. This increases the water content of the syngas from essentially zero (GAS-109) to 41.6 mol% (GAS-201), giving a steam to carbon monoxide ratio of 1.86 prior to entering the HTS reactor (R-203). The temperature of the gas stream also increases across these two "saturator" units, from roughly 69 °C (GAS-109) to approximately 195 °C (GAS-201). Further preheating of this gas stream is achieved in heat exchanger E-211 such that the gas enters the first HTS reactor (R-203) at 300 °C. The first HTS reactor is designed such that about 70 % of the entrant carbon monoxide (on a molar basis) is consumed; this results in the gas stream (GAS-203) leaving at a temperature of roughly 455 °C.

The shifted syngas in stream GAS-203 is cooled by means of a heat recovery system such that it enters the second HTS reactor (R-204) at 300 °C. This reactor reduces the carbon

monoxide content of the exiting stream (GAS-206) to about 15 % (on a molar basis) of the stream entering the first HTS reactor (GAS-202); the temperature of the stream leaving the second HTS stage (GAS-206) is approximately 335 °C. More heat is recovered from the shifted syngas in stream GAS-206 by means of a heat recovery system such that the shifted syngas enters the LTS reactor at 220 °C. The final carbon monoxide shift reactor reduces the carbon monoxide content of the shifted syngas gas stream (GAS-213) that leaves the unit to roughly 4 % (on a molar basis) of that entering the first HTS reactor (GAS-202). Further heat recovery is carried out on the shifted syngas gas stream such that the temperature of the stream sent to the cooling and drying unit (GAS-213) is about 110 °C.

Both the HTS and LTS reactions are highly exothermic and hence the overall efficiency of the Timmins Process is influenced significantly by effective heat integration in this unit. The first saturator column, C-200, receives water heated by direct contact with a proportion of the hot gas that leaves the LTS reactor (GAS-210a) in a "desaturator" column, C-201 (7 theoretical stages). Water make up in this recirculating system is achieved by using condensate extracted from GAS-213 by the drying unit.

The second saturator column, C-202, is heated in a more complex fashion. Firstly, a recirculating water loop (WAT-216, WAT-217 and WAT-218) is employed, with heat input being provided indirectly by heat exchanger E-213 that uses IP steam as a utility. Condensate from this heat exchanger is then either used directly as a saturator feed (WAT-214), or to heat returning sour condensate from the dehydration unit (WAT-311) in heat exchanger E-215 that, in turn, is fed to the saturator (WAT-215).

The IP steam that is used by E-213 derives from two sources; a "waste product" (WAT-208) from heat recovery carried out over the entire shift reactor system and from a direct IP steam bleed from the steam turbine on the power island (WAT-209). The reactor heat recovery system takes 65 bara BFW from the HRSG (WAT-203), passes the water through two stages of preheat in heat exchangers E-207 (exit of LTS reactor) and E-206 (exit of second HTS reactor) before raising steam in boiler E-209 (entrance to second HTS reactor) and superheating the steam in E-210 (exit of first HTS reactor). This superheated steam is then used to generate mechanical work in steam turbine K-212, where the steam pressure is dropped from 62.2 bara to 17 bara; an isentropic efficiency of 75 % was used for this turbine. It is the 17 bara steam leaving the turbine (WAT-208) that can be considered to be the "waste product" of the heat recovery system that is used to supply roughly 73 % (on a molar basis) of the steam to heat exchanger E-213. There is a strong incentive to minimize the amount of steam bled directly from the

steam turbine on the power island since it is preferably used to drive the steam turbine and raise mechanical work.

Two other items of heat integration exist in the carbon monoxide shift unit. Firstly, the syngas preheat for the first HTS reactor, carried out in E-211, uses HP BFW from the HRSG; this is supplied at 130 bara and 328 °C. The reactor preheater drops the temperature of this BFW to roughly 208 °C (WAT-201). In order to minimize the impact of this colder BFW returning to the HRSG, some additional heat recovery can be carried out in heat exchanger E-208, where the returning HP BFW is raised in temperature to 223 °C. The final item of heat recovery in this unit is to use the waste heat in the portion of the shifted syngas leaving the LTS reactor that is not routed to the desaturator column (GAS-210b) to act as a heat source to warm the rich DEPG in the AGR unit; this is carried out in heat exchanger E-217.

Cooling And Drying Unit

The objective of the cooling and drying unit was to remove excess water from the syngas leaving the carbon monoxide shift stage such that water ice was not formed in the cryogenic unit. The Peng Robinson thermodynamic model was used to model the interaction of the various components within this unit and a process flow diagram is shown in Figure S3.

The incoming shifted syngas (GAS-213) was cooled to 90 °C in heat exchanger E-300. Liquid water was collected in flash vessel V-301 and the shifted syngas stream (GAS-301) was then further cooled to 30 °C by means of heat exchanger, E-302. Further liquid water collection took place in flash vessel V-303. Cooling the syngas in this manner results in about 99 % (on a molar basis) of the water vapor being removed as condensate. This condensate is, however, mildly acidic (“sour”) due to it having been in contact with relatively high concentrations of carbon dioxide; it is, therefore, unsuitable for steam raising but it can be used as a source of make-up water in the two saturator systems in the carbon monoxide shift unit. 22 % (on a molar basis) of the condensate is heated from roughly 80 °C to 163 °C in heat exchanger E-308, using HP BFW from the HRSG as a utility, and returned to the first saturator system as make-up water. The balance of the sour condensate is split between the second saturator circuit (WAT-311) and a sour water drain (WAT-312).

The remainder of the water in the syngas stream (GAS-303) is removed in a desiccation system that is represented on the flowsheet by unit D-304. This is assumed to be a system supplied by a third party vender, such as a molecular sieve, and hence detailed modeling is not undertaken for this study. The energy required by this unit is estimated from existing industrial databanks[5].

Cyrogenic Unit

The fourth and final unit in the Timmins Process is the cryogenic unit that liquefies roughly 52 % (on a molar basis) of the carbon dioxide that is present in the dried, shifted syngas that leaves the cooling and drying unit (GAS-304). The cryogenic unit consists of a series of multi-stream PFHEs that are primarily cooled by a pre-cooled propane refrigeration cycle but are also tightly heat integrated to increase the overall efficiency and coefficient of performance. Based on the work discussed in Section 2.2, the Peng Robinson equation of state is used to model the thermodynamics of the gas mixture both in the vapor and liquid states. A process flow diagram of the cryogenic unit is shown in Figure S4.

The dried, shifted, syngas coming from the cooling and drying unit first passes through centrifugal compressor K-400. This unit recompresses the syngas from just below 30 bara back to 36 bara to compensate for the accumulated pressure drop through the Timmins Process up to this point; within UniSim the compressor was assumed to have an isentropic efficiency of 75 %. The gas stream leaving the compressor (GAS-400) is cooled from roughly 51 °C to 30 °C by heat exchanger E-401, which is assumed to use CW as a utility stream.

The syngas then passes through three stages of cooling and carbon dioxide liquefaction; the first stage consists of one multi-stream PFHE (E-402) whereas the remaining two stages each consist of two multi-stream PFHEs (E-404 and E-405; E-407 and E-408); these stages are split in order to assist heat recovery. Flash vessels follow each liquefaction stage such that liquid carbon dioxide can be recovered and the gas stream can be sent to the next liquefaction step. The PFHEs in each stage are specified to have a minimum temperature approach of 3 °C[2]. The proportion of carbon dioxide removed in each liquefaction step is shown in Table S2; almost 52 % (on a molar basis) of the carbon dioxide entering the cryogenic stage from the cooling and drying unit is removed by the liquefaction process.

The gas that leaves the final flash vessel (GAS-440) has a temperature of -38 °C; this stream, therefore, is used as an additional source of cold within the first and second liquefaction step (E-402 and E-405 respectively) to reduce the overall refrigerant flow, hence, the overall parasitic power load. Prior to re-entering the AGR unit, the gas stream leaving the first liquefaction step (GAS-442) is cooled from 27 °C to 16 °C in heat exchanger E-417, using liquid carbon dioxide as a utility. Pre-cooling the gas stream in this manner increases the energy efficiency of the AGR unit.

Further cold recovery can be achieved by passing the liquefied carbon dioxide back through selected PFHEs in the liquefaction process. When designing this system, it is crucial to ensure that the liquid carbon dioxide does not change phase; pumps P-410, P-411, P-412, P-413, P-414, P-416 and P-426 are specified for this purpose. Additional cold recovery takes place between the liquefied carbon dioxide stream (CO2-422) and the liquid propane stream (PRO-461) in heat exchanger E-415.

The primary refrigeration source to each PFHE is supplied by a pre-cooled propane cycle that used CW to drive the phase change of the propane from gas to liquid (using E-418). The temperature of the liquid propane (PRO-461) was assumed to be 30 °C, hence requiring a pressure of 10.8 bara; this temperature was dropped to -30.2 °C by heat recovery with the returning gaseous propane stream (PRO-487) and the liquefied carbon dioxide (CO2-422). The propane was split into three circuits, as detailed in Table S3.

The propane flowrate into each PFHE was adjusted such that a complete propane phase change was just attained across the unit. This ensured that the minimum amount of propane was used. Once the propane had passed through a PFHE, it was recompressed back to 10.8 bara in a series of stages, with intermediate compression steps specified such that the five gaseous propane streams could be recombined without any pressure loss. All compressors in the refrigeration cycle were assumed to operate with an isentropic efficiency of 75 % and all PFHE units were assumed to have a minimum approach temperature of 3 °C.

MODELING THE POWER ISLAND

The power island modeled for this study was based on that used in case 6 of the DoE studies[6] and consisted of two GE 7F gas turbines adapted for use with a humidified high hydrogen fuel. Exhaust gas from each turbine was passed through a dedicated HRSG with steam from the two HRSGs being combined and supplied to a single steam turbine. For simplicity, one HRSG was modeled, with its capacity being doubled. Specific process details surrounding the exact configuration and operating efficiencies of gas and steam turbines, along with combustion conditions were not given in the DoE study, hence this missing information was reconciled where possible an existing industrial study[5] and some literature data[7]–[9].

Data from a similar, existing, industrial study[5] was used to construct the initial UniSim power island model, with this model being subsequently refined to suit the needs of the Timmins Process. Specific data from the industrial study that was used included the optimal fuel gas flowrate to the turbines, an approximate but representative compressor and expander arrangement for a GE 7F turbine and a steam turbine, typical net power outputs from both gas

and steam turbines and a typical HRSG arrangement. These data were used to create an approximate stand-alone model of a representative IGCC power island within UniSim. Once this model was converged various process parameters, such as the turbine isentropic efficiency, were tuned such that the two cases matched. One this match had been attained, all heat and mass flows were fully integrated with the UniSim model for the Timmins Process and modifications made to the layout of the HRSG and to the steam bleeds on the steam turbine to account for the steam requirements that were specific to the Timmins Process.

The difference between the optimal flowrate of fuel gas required for the gas turbines and that produced by the Timmins Process was reconciled by linear scaling. Steam and water mass flows exported from the power island to the Timmins Process were linearly scaled up and as were the overall mechanical energy requirements of the Timmins Process such that energy consumption figures could be directly compared to those from DoE case 6[6], which used an essentially identical set of GE 7F gas turbines. All model results reported in this section were obtained by using UniSim R400 with the Peng Robinson equation of state for the process streams and the ASME steam thermodynamic model for all streams containing only water.

Humidifier And Gas Turbines

The composition and molar flow of feed gas that was initially found to be optimal[5] for the GE 7F gas turbines is shown in Table S4.

The fuel gas molar flowrate for the turbines is roughly 4 % higher than that produced by the Timmins Process, hence the subsequent scale factor that was used when integrating the water and steam flows from the power island to the Timmins Process was set to 5.5 % to include a margin for error. The same factor was used to scale up the energy requirements due to the Timmins Process; the optimal gas flowrate, however, was used within the power island modeling within UniSim.

Case 6 of the DoE studies incorporate a nitrogen flow into the turbines such that NO_x formation is limited[6]. The conditions of the diluent stream were duplicated from the DoE study such that it contained 99.3 mol% nitrogen, 0.5 mol% oxygen with a balance of argon; this stream entered the gas turbine at 93 °C and 26.5 bara. The flow rate of the diluent gas was adapted for the specific composition and flow of the fuel gas from the Timmins Process and data from the existing industrial study suggested that a flow of 7610 kmol/hr was required.

The exact processes in this unit were not modeled in full, with the model being created with sufficient detail to only account for the steam requirements and energy outputs of this operation. The combustion reaction was very simply modeled as the complete combustion of

the hydrogen, carbon monoxide and methane that was present in the fuel gas stream; within UniSim this was represented by a conversion reactor attaining 100 % conversion. An approximate process flow diagram of the humidification unit and of the gas turbines is shown in Figure S5.

Entrant fuel gas from the Timmins Process (GAS-500) was humidified and heated prior to combustion; the process used LP steam from the HRSG and IP steam from the steam turbine to perform this duty. This process was known to make use of both direct and indirect heat exchange; the model was created such that the required amount of steam[5] was directly injected into the fuel gas and that indirect heat exchange raised the fuel gas to the required temperature thereafter. The humidification system shown can only be considered a "short cut" approach, with the full system likely to consist of a more complex saturator system such as that modeled for the carbon monoxide shift unit within the Timmins Process. The humidified fuel gas (GAS-503a) was combined with compressed air in a conversion reactor (R-505, R-511), where the temperature rose to roughly 1330 °C. The combustion products (GAS-505a, GAS-505b) were dropped slightly in pressure (by 0.93 bar across VLV-506, VLV-512) to account for losses due to the flow path within the gas turbine, and subsequently combined with compressed air (AIR-535a, AIR-535b) and expanded through a turbine (K-507, K-513). The gas exiting the gas turbine was predicted to be at a temperature of 603 °C; due to the simplifications and assumptions in the model in this section, this was found to be an over-prediction when compared to both DoE case 6 and the existing industrial study[5], [6]. A cooler (E-508, E-514) was added as a simulation convenience to provide the outlet gas to the HRSG at a temperature of 533 °C.

The mechanical work provided by the gas turbine drove an air compressor that would physically exist on the same shaft (K-504, K-510). This compressor took air at 15 °C and 1 atmosphere pressure with a water content of 1.04 mol% and compressed it to 18.6 bara. The compressed air flow was split, with 10.6 % of the flow bypassing the combuster (AIR-535a, AIR-535b) and the balance being fed to the combuster. A small pressure drop, 0.01 bar, was included upstream of the air compressor to account for the accumulated pressure drop of the air flowing through filters and louvers.

In order to obtain a realistic output power from the combined compressor and turbine units, the isentropic efficiency was of each unit was adjusted such that the net expansion power (turbine power less compressor power) matched existing data[5]. Overall gas turbine data is shown in Table S5 and is comparable to values reported in the literature[7], [8].

Heat Recovery Steam Generator (HRSG)

Exhaust gas from the gas turbines is used to raise steam in the heat recovery steam generator (HRSG). The sparing policy for case 6, and hence for this study, is that each gas turbine is equipped with its own HRSG, with the steam flows from these HRSGs being combined to feed the steam turbine. For simulation purposes, the HRSG was modeled as one combined unit.

The HRSG contains economizers, boilers and superheaters for intermediate pressure (IP, 36.2 bara) and high pressure (HP, 134.2 bara) steam circuits, both of which are used directly in the steam turbine. The HRSG also contains reheaters for IP steam that is essentially the exhaust from the HP steam turbine; this allows an increased amount of work to be extracted from the IP and LP steam turbine stages. Within the HRSG there is also a economizer and boiler for low pressure (LP, 5 bara) steam; LP steam is used as a utility within the Timmins Process and within the gasification island. A process flow diagram for the HRSG is shown in Figure S6.

Care was taken when modeling the HRSG that the minimum temperature approach did not fall below pragmatic values. Literature[10], [11] suggests that a lower bound on the pinch temperature in an HRSG is about 6 °C. The distribution of water and steam flows to and from the HRSG is shown in Table S6.

Steam Turbine

The steam turbine in DoE case 6 consists of a HP, IP and LP section on a common shaft that is connected to a 24 kV synchronous alternator[6]; a similar piece of turbomachinery is therefore used in the current study. Steam exhausted at the exit of the HP section, at 344 °C and 32.9 bara is passed back to the HRSG to be superheated to 512 °C. The steam turbine used with the Timmins Process also has to provide steam at 52 bara to the gasifier and 20 bara to the IP steam header for use with the gasifier, fuel gas humidifier and as a heat source in the second saturator within the carbon monoxide shift unit.

For simulation purposes, the steam turbine was subdivided into five units, with steam bleeds being taken from the exit of each of the turbine sections. Additional steam bleeds at all three pressure levels were taken for use as steam seals for the turbine shafts; these bleeds are labeled as “leaks” in the process flow diagram. Additional HP boiler feed water was imported from the HRSG to desuperheat the 50 bara steam bleed. A process flow diagram for the steam turbine is shown in Figure S7 and a table showing the ancillary flows to and from the steam turbine is

given in Table S7. Note that the "LPS leakin" figure shown in this table along with the mass flowrates of steam for steam seals was taken from an existing, similar, case study[5].

The isentropic efficiencies of the steam turbine system were adjusted to attain outlet temperatures comparable to those from the existing case study[5] and are similar to those available in the literature[9]. The net power output of the system was then compared to the existing case study and the small difference between them accounted for as an additional mechanical loss. Finalized steam turbine mechanical data is shown in Table S8.

PERFORMANCE OF THE TIMMINS PROCESS

With regard to the AGR unit, the flowrate of DEPG around the absorption / regeneration loop was minimized with the objective of obtaining a minimum of 90 % carbon capture (referenced to the molar flow of carbon dioxide entering the Timmins Process in the syngas) subject to the constraint of the temperature of the DEPG entering the absorber not being less than -10 °C; this figure was chosen as a rough rule of thumb[12] based upon a margin of safety to avoid the temperature at which DEPG and water mixtures become slushy (-18 °C[13]). Lower DEPG flowrates result in lower pumping duties within the DEPG recirculation pump, P-108, in addition to smaller absorption and regeneration tower diameters. With a DEPG temperature of -6 °C, a DEPG flowrate of 15800 kmol/hr was required, giving a ratio between the molar flow of carbon dioxide in the absorption tower and the DEPG flow of 1.73. There is scope for more rigorous optimization to be carried out, which forms part of the future work originating from this study.

The two refrigeration cycles within the Timmins Process, embedded with the cryogenic unit and the AGR unit, are likely to be large consumers of mechanical energy. Initial analysis of the performance of these cycles for the "base case" process reveals a coefficient of performance (CoP) of 4.17 and 4.12 respectively. Scope for improving these CoPs further will be subject of a future study.

The Timmins Process requires a significant amount of heat to be imported from both the steam turbine and the HRSG. It is, therefore, imperative to ensure that the pinch temperatures within the HRSG are above typically accepted minimums. Literature[10], [11] suggests that a minimum pinch temperature of 10 °F, or about 6 °C, can be assumed when finned evaporator tubes are used. The composite curve for the HRSG that corresponds to the "base case" process is shown in Figure S8 with a plot of the pinch temperatures for each exchanger element being shown in Figure S9.

The data presented in Figure S8 and Figure S9 show that the pinch temperature within the HRSG is 7.2 °C within the IP and HP economizer. This is just above the lowest recommended temperature of 6 °C. It is suggested that the HRSG may need minor reconfiguration in order to increase the pinch temperature and to increase its robustness against process upsets.

The net plant HHV efficiencies were calculated assuming that the as-received higher heating value (HHV) of Illinois number 6 coal was 27113 kJ/kg[14]. The specific primary energy consumption for CO_2 avoided (SPECCA)[15] values were calculated according to Equation (2) and used the lower heating value (LHV) of Illinois number 6 coal, which was taken to be 26151 kJ/kg.

$$SPECCA = \frac{Q - Q_{ref}}{E_{ref} - E} \tag{2}$$

In Equation (2), Q is the heat rate of IGCC with embedded Timmins, expressed in units of kJ (LHV) per kilowatt-hour of electricity; Q_{ref} is the heat rate of DoE case 5[6] evaluated at the LHV of Illinois number 6 coal; E is the emission rate of CO_2 from IGCC with embedded Timmins, expressed in units of kg_{CO2} per kilowatt-hour of electricity and E_{ref} is the CO_2 emission rate from DoE case 5.

NOMENCLATURE

Roman Letters

E	CO_2 emission rate	$kg_{CO2}\ kWh_{el}^{-1}$
k	Rate constant	-
K	Equilibrium constant	-
r_{CO}	Rate of CO consumption	lb mol CO consumed per hr per lb catalyst
Q	Plant heat rate	$kJ_{LHV}\ kWh_{el}^{-1}$

Script and Greek Letters

$\mathcal{P}$	Pressure	atm
$\mathcal{T}$	Temperature	Rankine
ρ_b	Catalyst bulk density	lb ft^{-3}
φ	Activity coefficient	-

REFERENCES

[1] D. Kubek, E. Polla, F. Wilcher, *Purification and recovery options for gasification*, UOP^{TM} LLP, Illinois **2000**.

[2] K. Thulukkanam, *Heat Exchanger Design Handbook*, CRC Press, Boca Raton **2013**.

[3] H. Rase, J. Holmes, *Chemical reactor design for process plants*, John Wiley & Sons, New York **1977**.

[4] Honeywell, *UniSim Design - Simulation Basis Reference Guide*, **2010**.

[5] I. Salmon, *Private communication*, **2012**.

[6] J. Black, *Cost and Performance Baseline for Fossil Energy Plants Volume 1: Bituminous Coal and Natural Gas to Electricity*, 2nd edition, DOE/NETL - 2010/1397 **2010**.

[7] WO2014055307, (**2013**), invs.: M. Coney.

[8] E. Catalanotti, M. Pourkashanian, *Carbon Capture: A Technology Assessment Evaluation of Performance and Cost of Combustion Based Power Plants with CO 2 Capture in the UK*, The Centre for Low Carbon Futures, Leeds **2012**.

[9] R. Sanjay, O. Singh, "Thermodynamic Evaluation of Advanced Combined Cycle Burning Hydrogen", *Proc. NHA Annual Hydrogen Conference*, National Hydrogen Association, Sacramento, CA, USA, **2008**.

[10] R. Kehlhofer, F. Hannemann, F. Stirnimann, B. Rukes, *Combined-Cycle Gas & Steam Turbine Power Plants*, 3rd edition, PennWell Books **2009**.

[11] V. Ganapathy, *Chem. Eng. Prog.*, **1996**, *August*, 32.

[12] C. Hodrien, *Private communication*, **2012**.

[13] R. W. Bucklin, R. L. Schendel, *Energy Prog.*, **1984**, *4*.

[14] M. Matuszewki, *Detailed Coal Specifications*, DOE/NETL-401/012111 **2012**.

[15] R. Anantharaman, O. Bolland, N. Booth, E. van Dorst, C. Ekstrom, E. Sanchez Fernandes, F. Franco, E. Macchi, G. Manzolini, D. Nikolic, A. Pfeffer, M. Prins, S. Revani, L. Robinson, *European best practice guidelines for assessment of CO2 capture technologies*, European Benchmraking Task Force, Milan **2011**.

LIST OF TABLES

Table S1. Expressions for the rate constant, equilibrium constant and activity factor for the carbon monoxide shift reaction[3].

	Catalyst type	
Parameter	**Iron (HTS)**	**Copper-zinc (LTS)**
k	$\exp\left(15.95 - \frac{8820}{\mathcal{T}}\right)$	$\exp\left(12.88 - \frac{3340}{\mathcal{T}}\right)$
K	$\exp\left(-4.72 + \frac{8640}{\mathcal{T}}\right)$ for $760 \leq \mathcal{T} \leq 1060$ $\exp\left(-4.33 + \frac{8240}{\mathcal{T}}\right)$ for $1060 \leq \mathcal{T} \leq 1360$	
φ	$0.816 + 0.184\mathcal{P}$ for $\mathcal{P} \leq 11.8$	$0.86 + 0.14\mathcal{P}$ for $\mathcal{P} \leq 24.8$
	$1.53 + 0.123\mathcal{P}$ for $11.8 < \mathcal{P} \leq 20$	
	4 for $\mathcal{P} > 20$	4.33 for $\mathcal{P} > 24.8$

Table S2. Details of the carbon dioxide liquefaction amounts within the cryogenic unit.

Heat exchanger	E-402	E-404	E-405	E-407	E-408
Proportion of carbon dioxide condensed from process stream (% molar of incoming carbon dioxide)	16.8	22.8		12.0	

Table S3. Propane flow rates, pressures and temperature for the cryogenic refrigeration cycle.

Heat exchanger	E-402	E-404	E-405	E-407	E-408
Propane pressure (bara)	1.55	1.25	1.25	105	105
Propane flowrate (kmol/hr)	3000	1705	1425	1265	615
Propane temperature (°C)	-32.0	-37.3	-37.3	-41.4	-41.4

Table S4. Fuel gas and humidified fuel gas condition and compositions for use in the gas turbines.

Fuel gas supplied to power island (GAS-500)			Fuel gas entering combuster (GAS-503a)		
Pressure	32.1	bara	Pressure	29.5	bara
Temperature	25.8	°C	Temperature	193	°C
Flow rate	17240	kmol/hr	Flow rate	half of 19370	kmol/hr
Component	Composition (mol %)		Component	Composition (mol %)	
Water	0.00		Water	10.93	
Carbon dioxide	1.45		Carbon dioxide	1.29	
Hydrogen sulphide	0.00		Hydrogen sulphide	0.00	
Hydrogen	87.67		Hydrogen	78.10	
Carbon monoxide	3.93		Carbon monoxide	3.50	
Nitrogen	5.92		Nitrogen	5.28	
Argon	0.97		Argon	0.86	
Methane	0.06		Methane	0.05	

Table S5. Gas turbine data used in the UniSim model.

Unit tag	**K-504**	**K-507**	**K-510**	**K-513**
Duty	**Compressor**	**Turbine**	**Compressor**	**Turbine**
Isentropic effiency (%)	80.35	87.29	80.35	87.29
Expansion work (kW)	-226600	471200	-226600	471200
Additional losses (kW)	1200		1200	
Net output gas turbine unit (kW)	243400		243400	
Mechanical efficiency (%)	98.69		98.69	
Mechanical output (kW)	240211		240211	
Pressure ratio	18.6		16.9	

Table S6. Flows of water and steam to and from the HRSG.

Pressure level	Total flow rate (tonnes /hr)	Direction of flow	Source / destination	Ancilliary flow (tonnes/hr)	Supply temperature (°C)	Location of use
LP (5 bara)	121.6	From HRSG	LP steam header	54.90	275	Case 5 LP steam requirement
		From HRSG	LPS to syngas humidifer	112.0	275	Timmins Process
IP (36.2 bara)	92.37	From HRSG	IPS to turbine	623.9	512	Steam turbine
		To HRSG	Exit of HP steam turbine	531.5	344	Steam turbine
HP (134.2 bara)	755	From HRSG	HPS to turbine	562.3	520	Steam turbine
		From HRSG	Desuperheating 51 bara steam from turbine	1.050	165	Steam turbine
		From HRSG	HP BFW to gasifier island	365.4	165	Case 5 HP BFW requirement
		From HRSG	HP BFW to CO shift heat recovery system	181.3	165	Timmins Process
		From HRSG	Condensate reheat in drying unit*	13.33	163	Timmins Process
		From HRSG	1st HTS reactor preheat in CO shift unit**	243.6	328	Timmins Process
		To HRSG	Condensate reheat in drying unit*	13.33	90	Timmins Process
		To HRSG	1st HTS reactor preheat in CO shift unit**	243.6	227	Timmins Process
		To HRSG	HPS grom gasifier island	358.0	331	Case 5 HPS generation

Table S7. Mass flows of steam from the steam turbine for non-energy raising uses.

Turbine stage	Pressure (bara)	Location of use	Ancilliary flow (tonnes/hr)	Temperature (°C)
HP	121	HPS leakage	9.72	518
	52.8	Gasifier	20.4	395
	35.9	IPS leakage	3.6	344
IP	20.7	Gasifier	12.6	454
		CO shift unit (2nd saturator)	68.9	454
		Fuel gas preheater	19.8	454
LP	4.76	Fed back to HRSG	62.4	264
		LPS leakage	0.628	264
		LPS leakin	3.08	264

Table S8. Steam turbine mechanical data.

Unit tag	K-700	K-701	K-702	K-703	K-704
Inlet pressure (bara)	120.9	52.78	30.38	20.65	4.76
Outlet pressure (bara)	52.78	35.88	20.65	4.76	0.07
Steam inlet temperature (°C)	518	395	511	454	264
Isentropic effiency (%)	85.46	86.49	88.48	91.14	93.11
Expansion work (kW)	33150	13550	20380	55330	86410
Additional losses (kW)	365	149	224	609	951
Net turbine output (kW)	32785	13401	20156	54721	85459
Mechanical efficiency (%)	98.5	98.5	98.5	98.5	98.5
Mechanical output (kW)	32293	13200	19854	53900	84177
Total mechanical output (kW)	203424				

LIST OF FIGURES

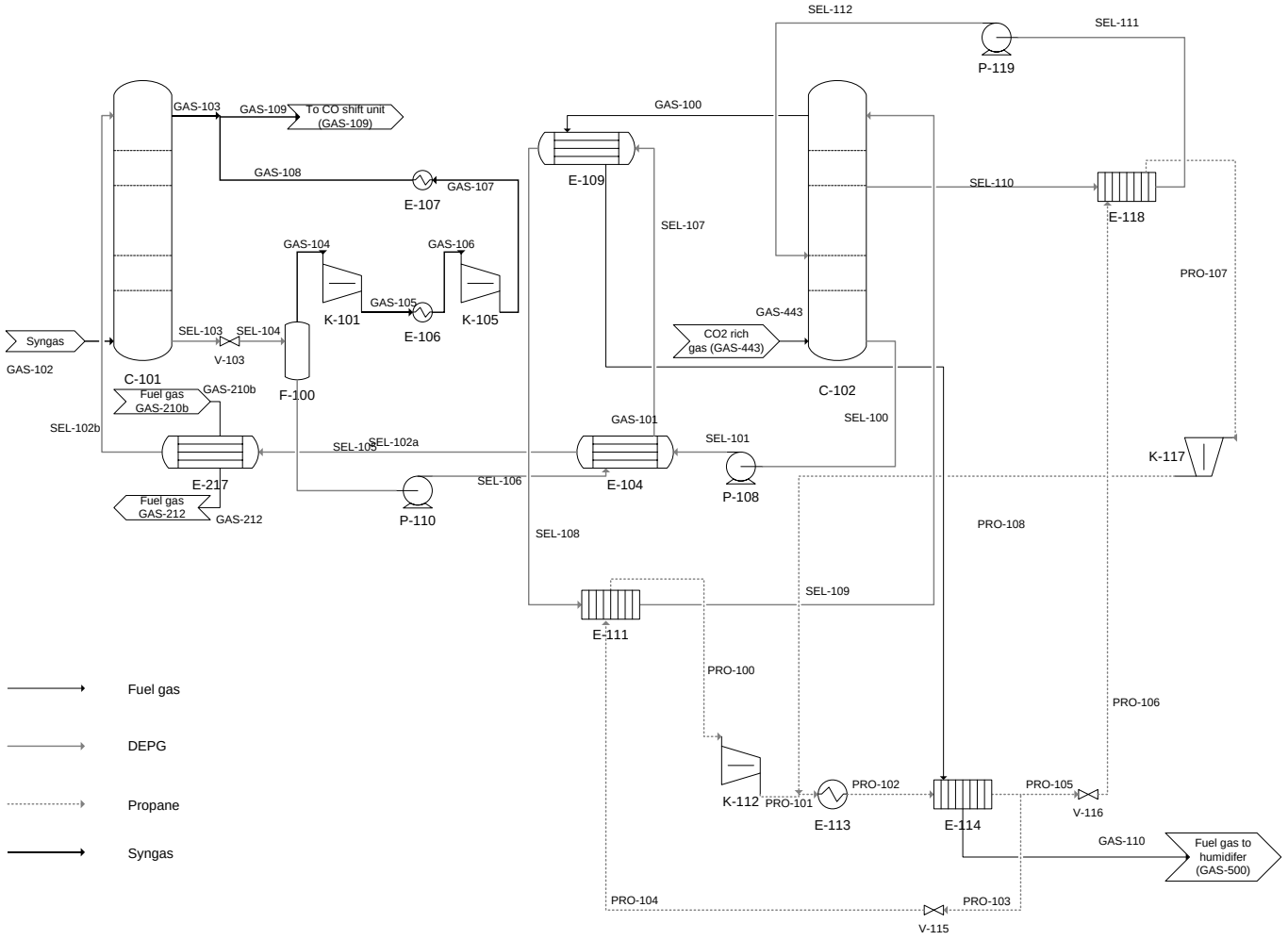

Figure S1. Process flow diagram for the AGR unit. Shell and tube symbols represent heat exchangers with a minimum approach temperature of 10 °C and plate and frame symbols represent heat exchangers with a minimum approach temperature of 3 °C.

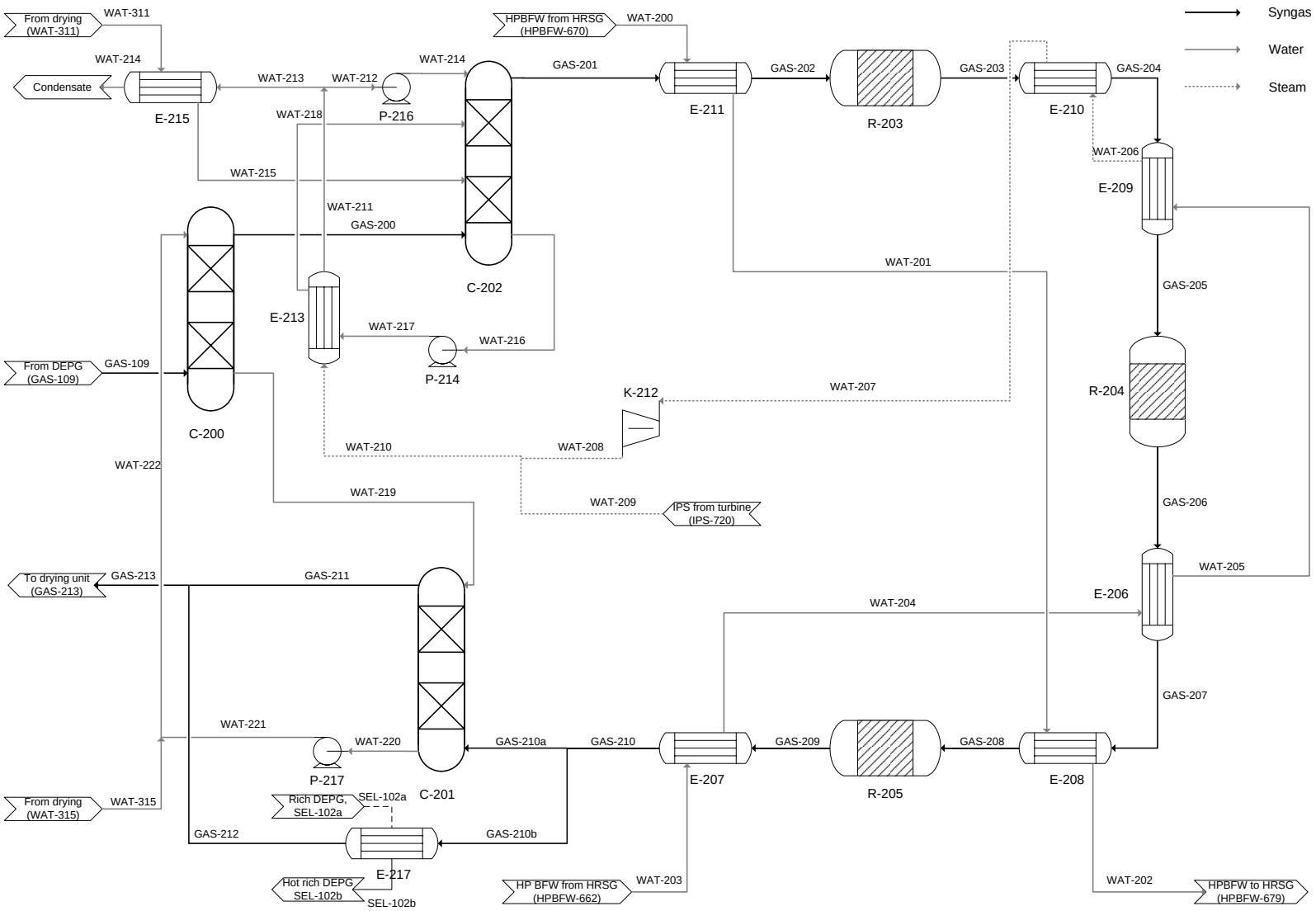

Figure S2. Process flow diagram for the carbon monoxide shift unit.

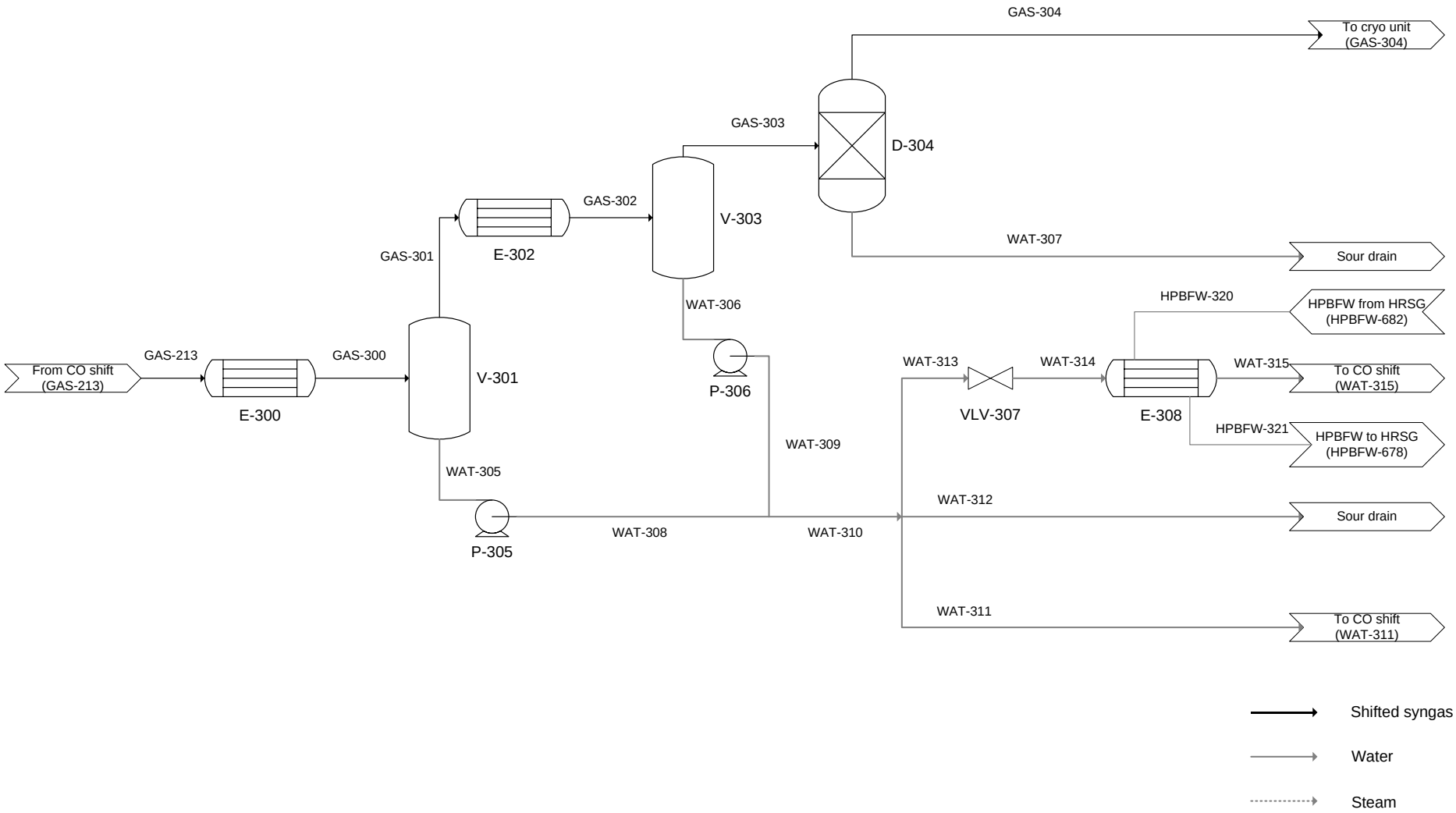

Figure S3. Process flow diagram for the cooling a drying unit.

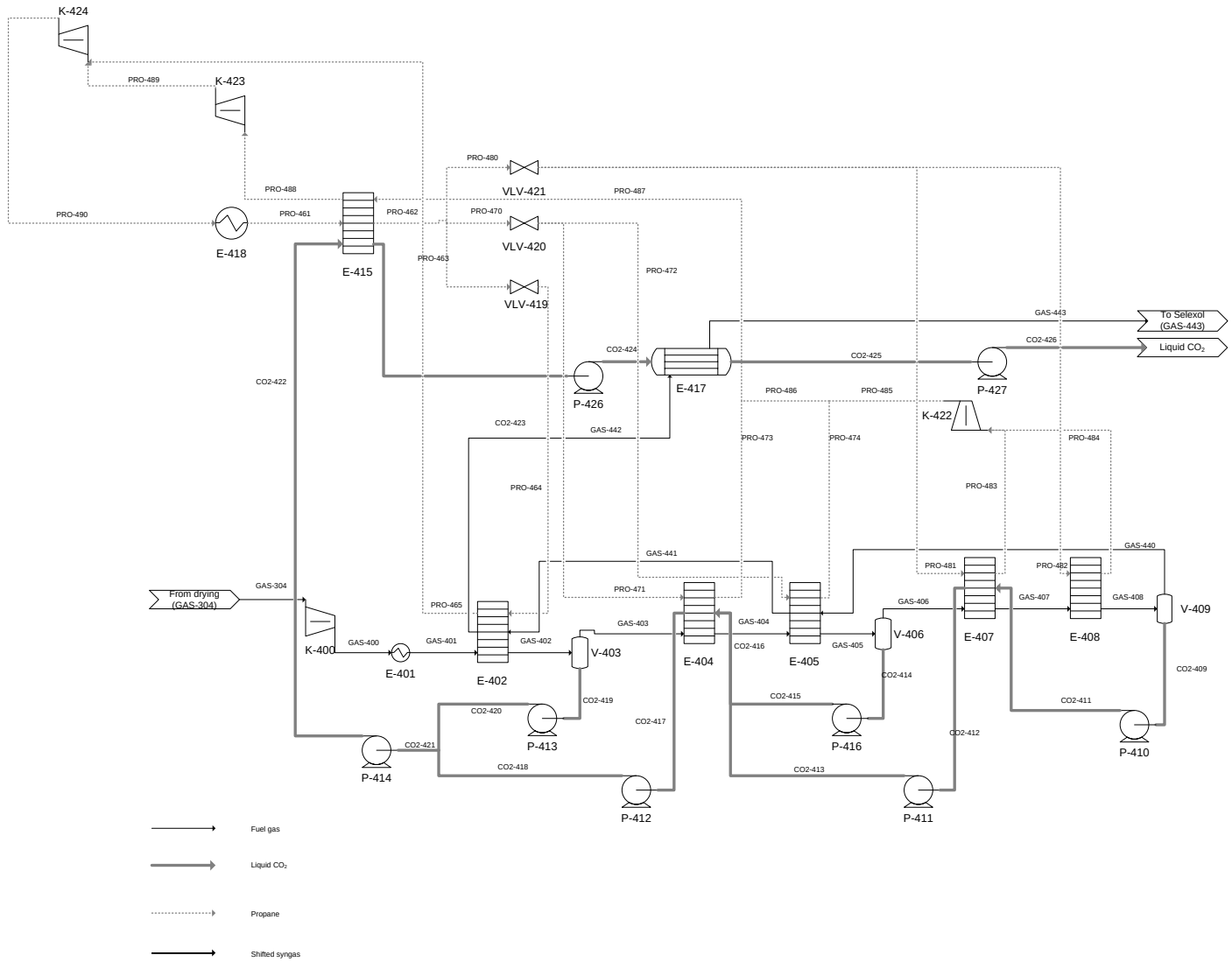

Figure S4. Process flow diagram for the cryogenic unit. Shell and tube symbols represent heat exchangers with a minimum approach temperature of 10 °C and PFHE symbols represent heat exchangers with a minimum approach temperature of 3 °C.

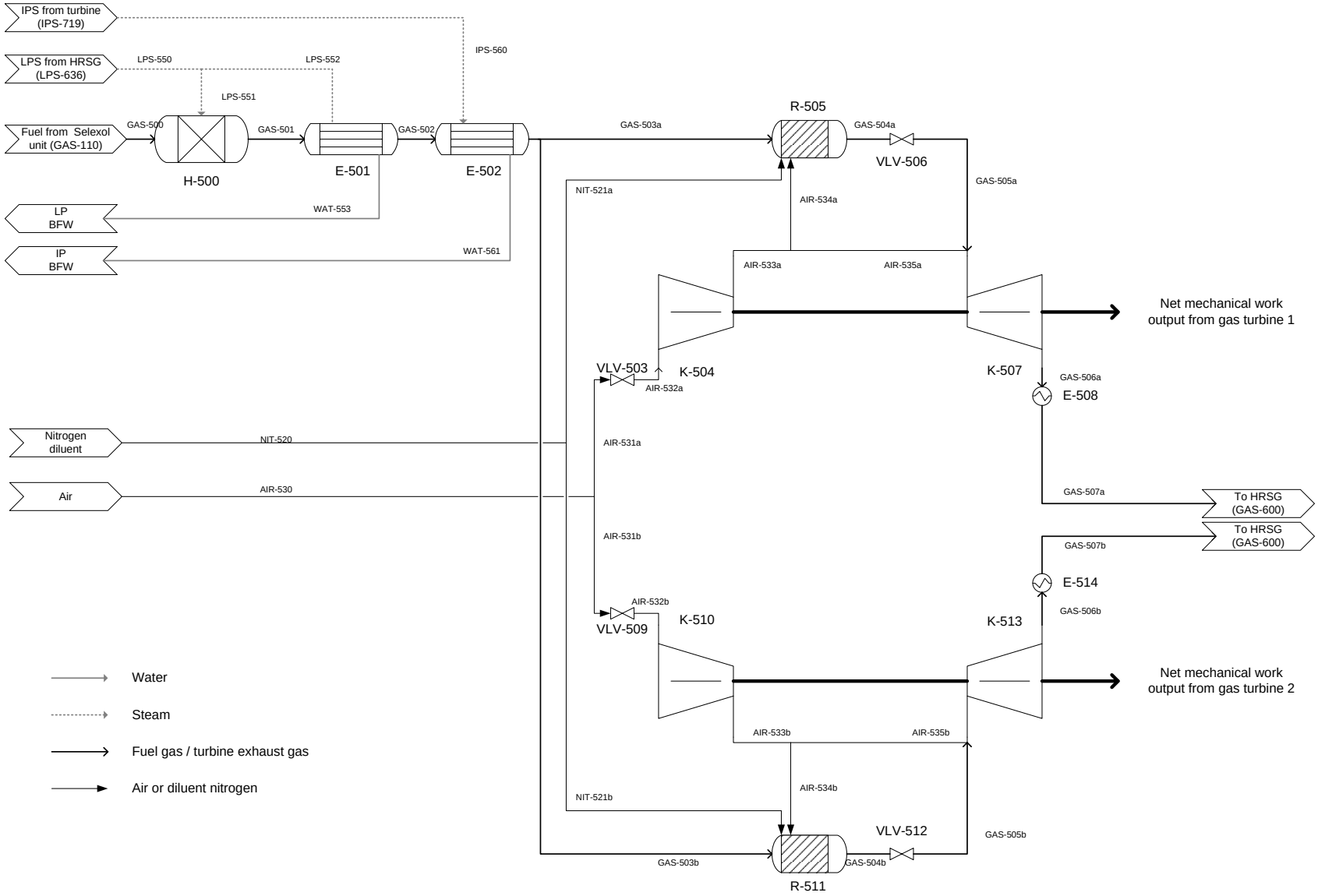

Figure S5. Process flow diagram of the approximate representation of the gas turbine and combustors

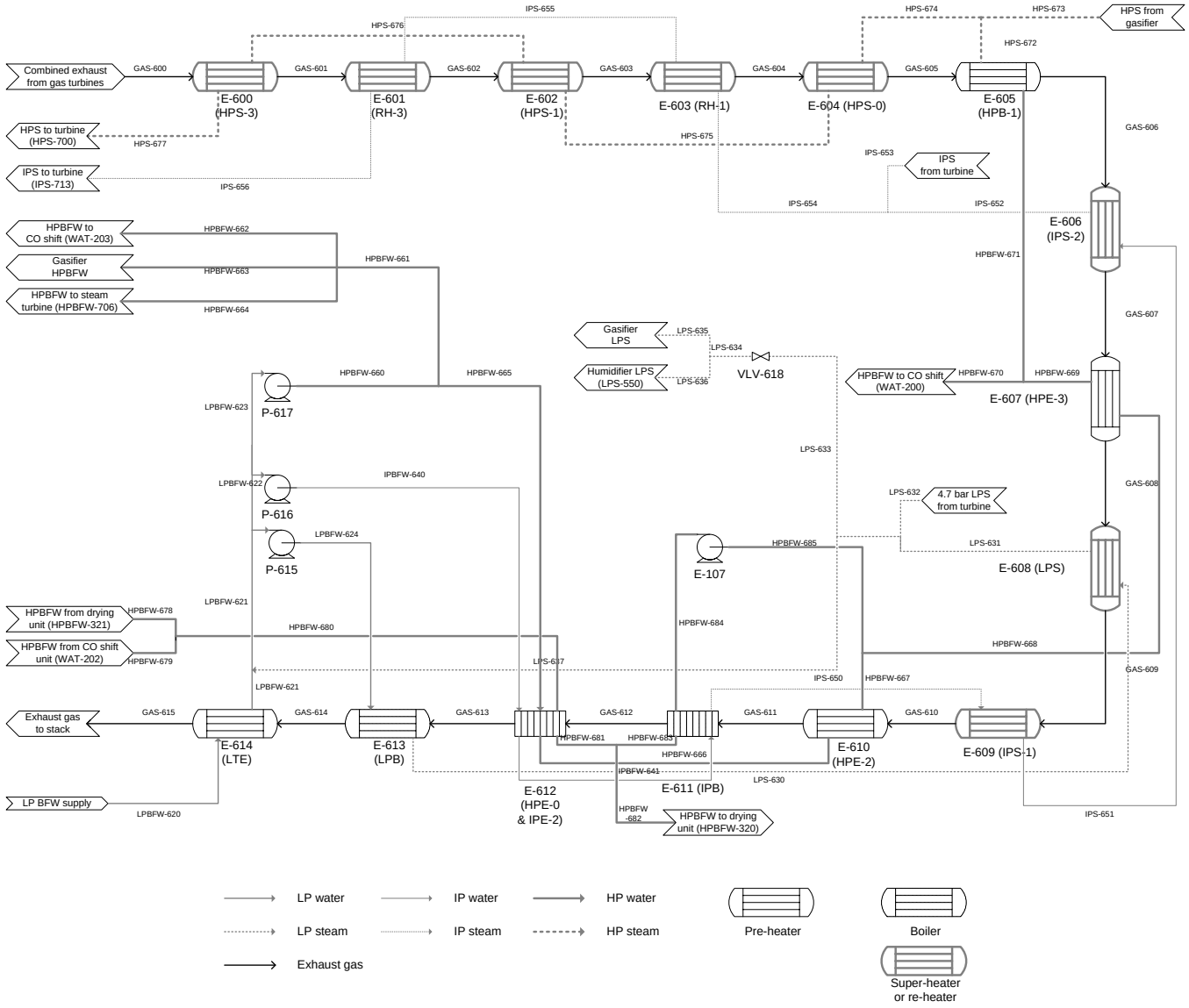

Figure S6. Process flow diagram for the heat recovery steam generator (HRSG).

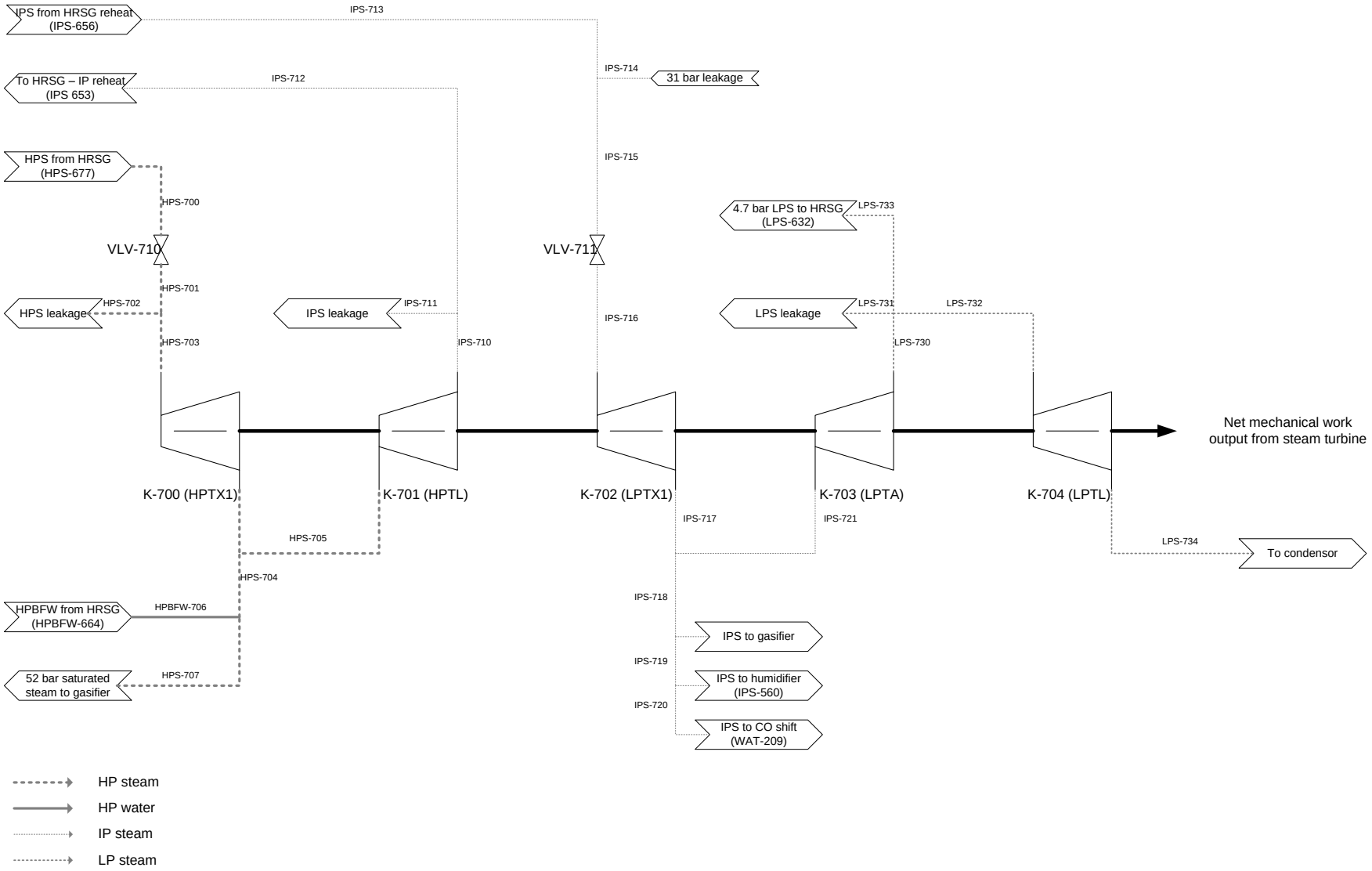

Figure S7. Process flow diagram for the steam turbine.

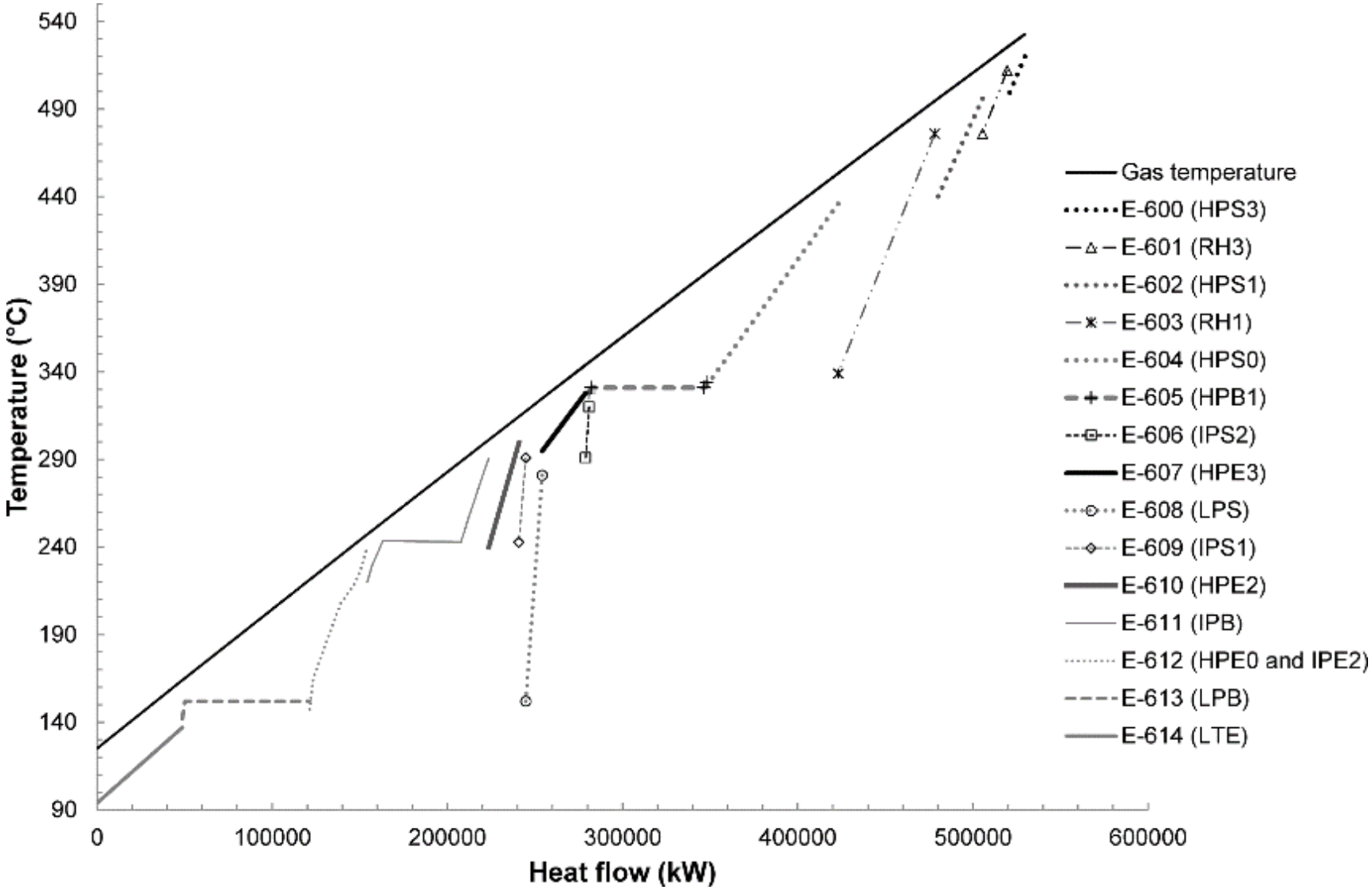

Figure S8. Composite curve for the HRSG.

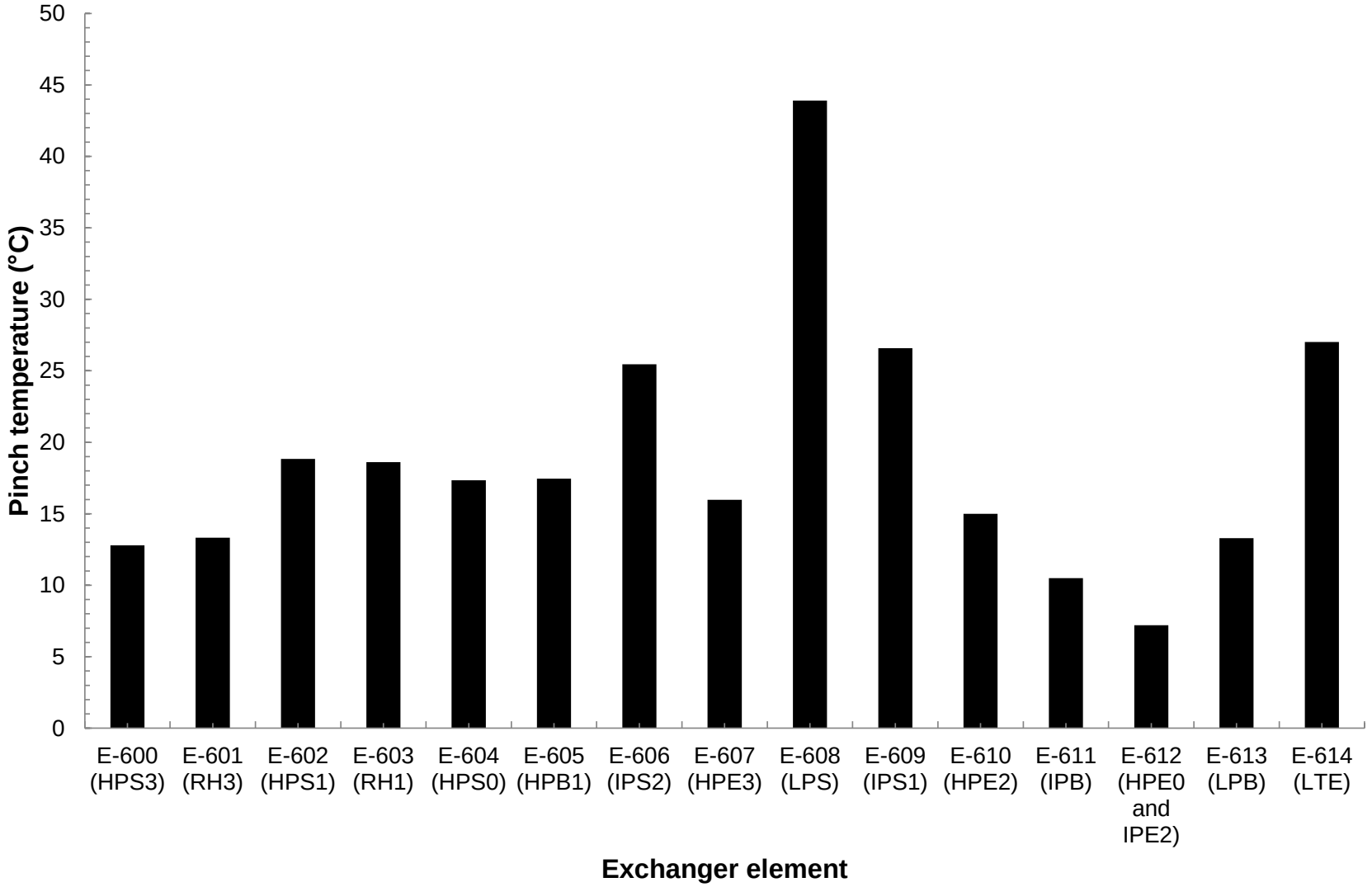

Figure S9. Plot of the pinch temperature within the HRSG as a function of exchanger element.